Non-linear climate dynamics

LPHYS2264

Lecture notes

2025–2026

Michel Crucifix

Faculté des Sciences

UCLouvain

Contents

1 The backround spectrum: (macro-)weather and climate regimes 7
- 1.1 Fluctuations and Variability Modes in Weather and Climate 8
  - 1.1.1 Fluctuation analysis of stochastic processes 8
  - 1.1.2 Stationary and non-Stationary stochastic processes 8
  - 1.1.3 Lovejoy's classification of regimes 11
  - 1.1.4 Flexibility of regime boundaries 12
  - 1.1.5 Self-Similarity and fluctuation regimes 13
- 1.2 Spectral description of variability 15
- 1.3 Fluctuation analysis revisited: Wavelets 17
  - 1.3.1 Fluctation spectrum is a wavelet specturm 17
  - 1.3.2 Link between fluctuation and power spectrum . . 18
- 1.4 Sythesis: what are climate regimes? 19

2 Stochastic EBMs 21
- 2.1 1-D EBM 21
- 2.2 2-D EBM 22

3 Linear waves 27
- 3.1 Basic notions 28
  - 3.1.1 Stability 28
  - 3.1.2 Wave equation 29
  - 3.1.3 Basic hydrodynamic equations 30
  - 3.1.4 Shallow-water model 32
- 3.2 Gravity waves 34
  - 3.2.1 Shallow-water gravity waves 34
  - 3.2.2 Setting initial conditions 35
  - 3.2.3 Capillary waves 35

3.2.4 Deep-water, barotropic, non-rotational gravity waves 36
3.2.5 Internal gravity waves 38
3.2.6 Accounting for stratification in a two-layer Saint-Venant model 39
3.2.7 Gravity waves in a closed channel 41
3.3 Quasi-hydrostatic waves in the f-plane 43
3.3.1 Vorticity equation in shallow water 43
3.3.2 Geostrophic velocity 43
3.3.3 Poincaré Waves (f-plane) 43
3.3.4 Kelvin waves 45
3.4 Quasi-geostrophic barotropic waves in the β-plane 47
3.4.1 Geostrophic wind in the f-plane 47
3.4.2 Geostrophic reference in the mid-latitude β-plane 47
3.4.3 Quasi-geostrophic flow in shallow-water 47
3.4.4 Quasi-geostrophic flow in pressure coordinates . . 49
3.4.5 TODO : Quasi-geostrophic flow in horizontal coordinates 51
3.4.6 Shallow-water rossby waves in the extratropical β-plane 51
3.5 Quasi-hydrostatic waves in the equatorial β-plane 54
3.5.1 Shallow-water equations in the equatorial β-plane 54
3.5.2 Equatorial Kelvin waves 55
3.5.3 Equatorial Rossby waves and other solutions . . . 56
3.6 Kelvin-Helmoltz instability 59
3.7 Baroclinic instability in the f-plane 63
3.7.1 Equations of a quasi-geostrophic perturbation with mean velocity shear 63
3.7.2 Two-layer quasi-geostrophic model 64
3.7.3 Philip's theory in pressure coordinates 67
3.7.4 Interpretation of the baroclinic field 68
3.7.5 Eady problem 68

4 Non-linear ocean-atmosphere phenomena 69
4.1 Beyond linearity with a modelling hierarchy 70
4.2 The Stommel two-box model 72
4.3 The Winton Oscillator 75
4.4 The El-Nino Southern Oscillation 77

4.5 The Vallis model : accounting for the Bjerkness feedback . 77
4.5.1 The Tziperman madel : chaos and synchronisation accounting for delayed feedbacks 81
4.5.2 Transition to Chaos 82

5 Non-normal growth **85**
5.1 The alternative paradigm: non-normal stochastic excitation 86

6 Climate dynamics **93**
6.1 Astronomical forcing 94
6.1.1 Elements of insolation theory 94
6.1.2 The planetary problem 98
6.1.3 The luni-solar precession 104
6.1.4 The climate modelling problem 104

Foreword

This course, LPHYS2264 builds upon a rich legacy of earlier iterations that focused primarily on *atmospheric waves and instabilities*. Much of the material presented in these notes originates from that foundational content. However, my own research and teaching experiences have broadened my perspective to encompass *climate instabilities* in a much wider sense.
The climate system is inherently dynamic, oscillating and fluctuating across an astonishing range of timescales—from minutes to millions of years. My objective in this course is to expand the traditional focus of the material to include this broader perspective. This involves introducing additional concepts, starting from the fundamental *definition of fluctuations* and extending to the methods used to identify and characterize them.
Ultimately, my goal is to develop a comprehensive set of notes organized around these key notions:

- **Periodic phenomena** and their underlying mechanisms,
- **Fluctuations** and their statistical characterization,
- **Modelling** these phenomena across all relevant timescales.

This course will also include a series of exercises, some of which will involve *coding and data analysis*, to deepen your understanding and practical skills. This is a long-term project that will evolve over the years, shaped by a collaborative effort between myself and the students. Together, we will refine and expand these notes, ensuring they remain relevant, rigorous, and engaging.
But at this point, these notes are fairly dry and lack illustrations and interpretation. This is evolving material, be patient. Here and there you will find some ”TODO”.

Chapter 1

The backround spectrum: (macro-)weather and climate regimes

1.1 Fluctuations and Variability Modes in Weather and Climate

When observing climate and weather, one can distinguish fluctuations that can be described statistically. On the one hand, there are phenomena occurring at specific periods or involving specific timescales. This duality allows us to approach these phenomena from two complementary perspectives: the statistical description of fluctations, and the analysis of their spectral signature.

1.1.1 Fluctuation analysis of stochastic processes

A stochastic process is, loosely speaking, a mathematical object that describes the evolution of a state variable according to probability laws. One of the great discoveries of early 20th-century physics is that some physical systems can be adequately described by stochastic processes. A classic example is Brownian motion, which is modeled as a random walk. Similarly, certain variables of the climate system can also be effectively described using stochastic processes.

1.1.2 Stationary and non-Stationary stochastic processes

Consider first a system that accumulates fluctuations over time without any restoring force. This can be described by the process mapping x at time t to its value a time δt later:

$$x_{t+\delta t} = x_t + \sqrt{\delta t}\, \eta_t,$$

where η_t is a random variable drawn form a normal (Gaussian) distribution. Such as process is non-stationary: there is no mechanism to prevent it from drifting, and it does not converge to any specific region of the state space over time. The map is called a 1-D randow walk, and it can be thought of as the discrete version of a continuous process called the Wiener process. We give here the differential notation because we will use it later on:

$$\mathrm{d}x = \mathrm{d}W_t$$

So $\mathrm{d}W_t$, the increment of a Wiener process, can be thought of as the expression of a random, normal-distributed increment but of amplitude $\mathrm{d}t$.

Because this is a randow walk, the expected difference, in absolute value, between two observations distant in time by ΔT *increases* proportionnaly to $\sqrt{\Delta T}$.
Now, consider that this same system is constrained by a restoring force that prevents it from drifting away. The dynamics will be akin of a linear relaxationg system whose differential eqpression would be

$$\mathrm{d}x = - - \frac{1}{\tau} x \, \mathrm{d}t,$$

but acconting for continuous disturbances. The equation describing the process is stochastic differential equation and is written:

$$\mathrm{d}x = -\frac{1}{\tau} x \, \mathrm{d}t + \mathrm{d}W_t.$$

This is a Ornstein-Uhlenbeck process and it can be simulated as follows: (based on Gardiner 2004, eqs. 3.8.72 and 3.8.73):

$$x_{t+\delta t} = e^{-\delta t/\tau} x_t + \sqrt{\frac{\tau}{2}\left(1 - e^{-2\delta t/\tau}\right)}\, \eta_t. \tag{1.1}$$

This discretised version is a case of finite-memory autoregressive process, whose more general form is $x_{t+\delta t} = a x_t + \sigma \eta_t$[1]
If the system is not observed long enough, its mean and average converge to finite and well defined values, which is characteristic properties of a stationary process. However, if it is observed over too short a time (sampling with $\delta t \ll \tau$ and observing over a time $\delta T < \tau$, it will rather behave as a random walk. A drift will generally be visible and which can be interpreted as the expression of non-damped accumluation of finite-amplitude fluctuations, as expected in a non-stationary process.
Therefore, for such a process, one can distinguish too "regimes", where the word "regime" is here used to depict a range of time scales over which the behaviour appears different. The difference betwene these two regimes by plotting the standard deviation of successive averages of the process

[1] say there is an abuse of notation.

over a time ΔT, and see how this variance evolves over time. We note this quantity $\langle|\Delta\bar{x}|^2_{\Delta T}\rangle^{1/2}$.
We will provisionnaly call the dependency of this variance of averages over ΔT, on ΔT the fluctuation spectrum. This notion will be refined later on (Sect. 1.3.1) but for the moment, observe how this quantity behaves depending on the regime.

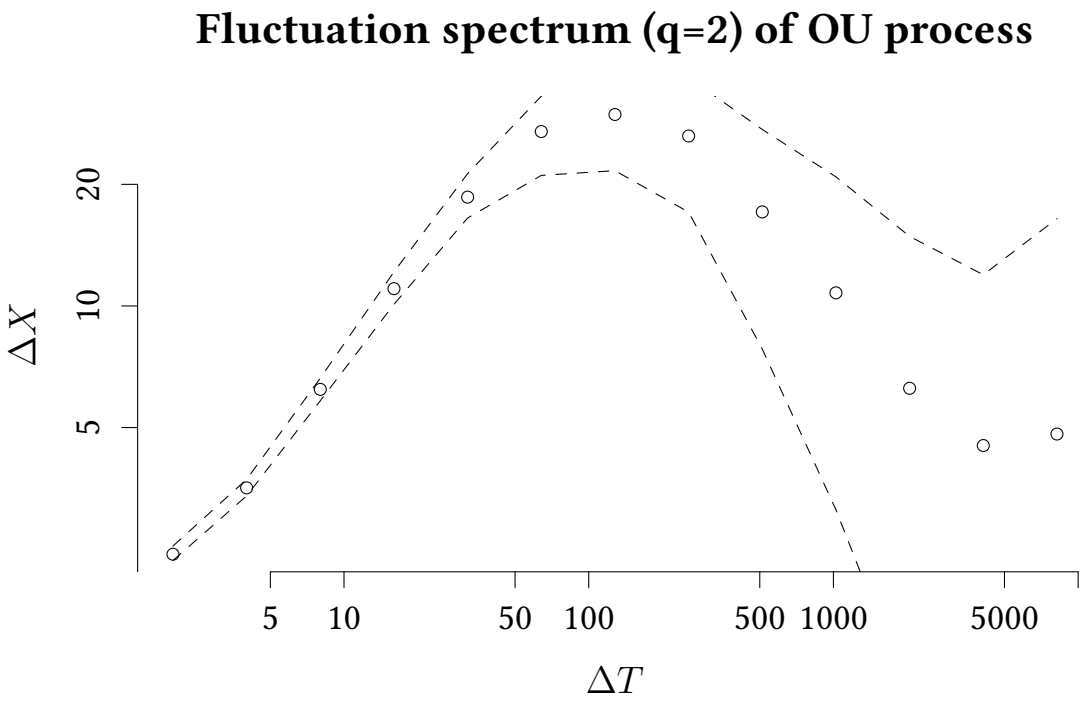

Figure 1.1: Average and quantiles of 100 realisations of a Orstein Uhlenbeck process, with δt=1, $\tau = 32$.

On can see that on timescales smaller than $2\pi\tau$, the size of fluctuations grows with the scale. The power-law, visible on the logarithmic plot, is $\langle|\Delta_{\bar{x}}|^2\rangle^{1/2} \propto \Delta_T^H$ with $H = 1/2$. The longer you observe the system, the larger the fluctuations you can register. On timescales much larger than $2\pi\tau$, fluctuations enter the averaging regime. These are the timescales for which it makes sense to ask about the average state of the system, as you have observed it for a sufficiently long time to estimate it accurately. In

this regime, $H = -1/2$.
The rule of thumb is to view regimes with $H > 0$ as "fluctuating" fluctuating regime (or "non-stationary" for these observation times), and regimes with $H < 0$ as "averaging" averaging regime, again for this observation time.

1.1.3 Lovejoy's classification of regimes

The fluctuating regime is characteristic of what we commonly call weather. For example, if you observe temperatures over five days, you can expect larger fluctuations than if you observe them over just two hours.
When observing weather over several years to several decades, a statistical description of weather typically emerges. This description includes well-defined averages, variances, and, more generally, meaningful distributions of events. While it might be conventional to call this the "climate regime," we prefer the terminology of S. Lovejoy and refer to it as macro-weather, a term inspired from statistical physics. The idea is that, within this time range, a "macroscopic" perspective on fluctuations becomes possible, allowing for the characterization of their variance, skewness, and other statistical properties. Drawing on the analogy provided by the Lorenz-Saltzman model Lorenz 1963, describing macro-weather would be akin to describing the attractor of the weather system. Macro-weather typically emerges on timescales greater than a few years. A canonical period for defining macro-weather is 30 years, though anthropogenic forcing introduces non-stationarity.
Lovejoy reserved the term "climate" to describe another fluctuating regime. Indeed, on timescales of several thousand years, changes in the carbon cycle and ice sheets generate new sources of positive feedback, which can again lead to growing fluctuations at larger timescales. Interglacial cycles are one example. These processes involve different physics and feedback mechanisms than those of weather, justifying the use of the term "climate dynamics" in a narrow sense to specifically describe these fluctuations. On timescales of several hundred thousand years, climate dynamics can be viewed from a macroscopic perspective: this would be the "macro-climate".
This macro-climate regime itself changes, hinting at the possibility of "mega-climate" fluctuation dynamics, for example, those associated with plate

tectonics and biological evolution.

HERE; EXPLAIN THAT THERE IS SOME JUSTIFICATION BASED ON EMPIRICAL DATA AND THAT IT IS A BIT SPECULATIVE

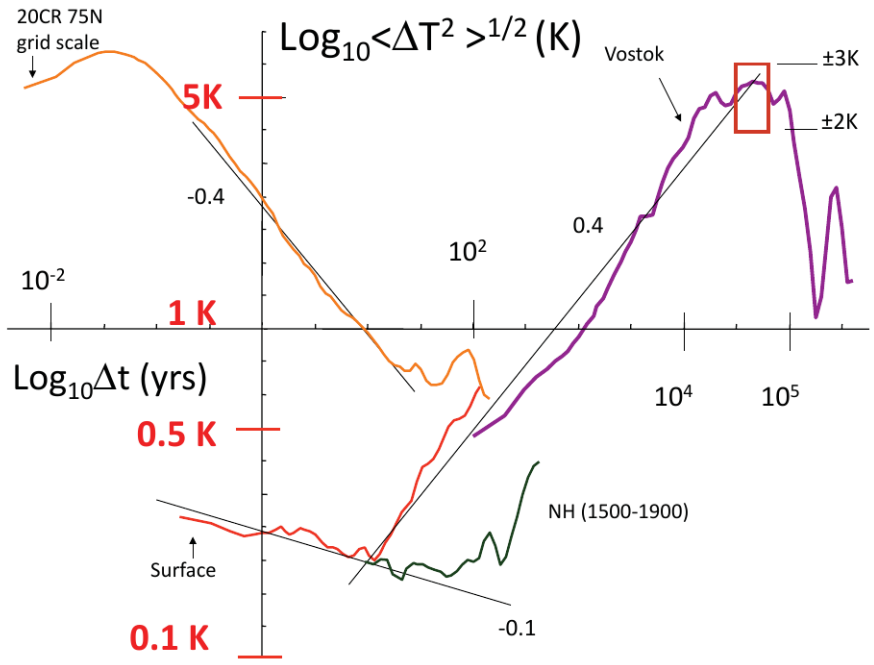

Figure 1.2: Fluctuation regimes in climate systems, as analyzed by Lovejoy, Schertzer, and Varon 2013

1.1.4 Flexibility of regime boundaries

The regimes and categories described here should not be viewed as rigid. The climate system encompasses a vast number of processes with diverse dynamics. Consequently, the boundaries between weather, macro-weather and climate are not so sharp; they may depend on latitude and also geological period. You do not expect the same dynamics and regimes in a cold period with ice-sheets, than during a hot period such as the Cretaceous or the Devonian.

1.1.5 Self-Similarity and fluctuation regimes

rather say there are two broad interpretations of the output of fluctuation analysis.

One key idea conveyed by the notion of a "regime" as illustrated by the fluctuation spectrum, is that at least over a certain range of timescales the system behaves consistently across that range. This consistency may manifest itself in statistics akin to those of a self-similar process. For example, the ratio of variances from timescale τ to 10τ is the same as the ratio of variances from 10τ to 100τ. How can this self-similarity arise? There are two broad family of explanations.
Ultimately, fluctuations originate from some form of excitation, often of thermal origin (as in Brownian motion). The critical question is how these fluctuations propagate to larger scales. We can sketch two broad families of processes that explain this propagation:

- **Accumulation of Fluctuations with Restoring Feedback:** Fluctuations accumulate but are damped by restoring feedbacks. For instance, the ocean, with its large thermal inertia, may accumulate thermal fluctuations of atmospheric origin, but on the some characteritic time scale these fluctations are damped by negative feedbacks restoring energy balance. Such systems typically exhibit an Ornstein-Uhlenbeck-type spectrum, as reviewed in Section 1.1.2. This forms the basis of Hasselmann's theory (Nobel Prize 2021), which can be extended to account for different ocean reservoirs or even a continuum of scales Lovejoy 2021. At its core, this is a linear theory — the self-similar characteristics of the times series are inherited from the self-similiar nature of the stochastic process. It is developed in Chapter 2.
- **Turbulent Processes:** Here, the system involves a large number of degrees of freedom, where structures of different timescales and spatial scales interact nonlinearly. These interactions are ultimately regulated at the microscopic level by balance equations. The similarity of the governing equations across scales leads to energy transfers that naturally produce fluctuation spectra with characteristic slopes, modelled by considerations based on dimension analysis and observations. A classical result due to Kolmogorov predicts that velocity fluctuations scale with space (not time) as $\Delta v \propto \Delta x^H$ with $H = 1/3$. Scal-

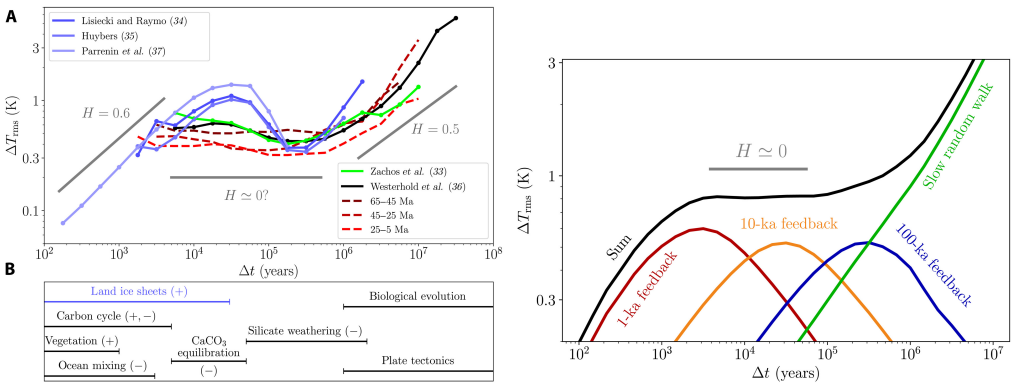

Figure 1.3: Figures from Arnscheidt and Rothman 2022, interpreting fluctuation regimes as signatures of the expression of dominance of positive feebacks ($H > 0$), amplifying fluctuations, and negative feedabck ($H < 0$), damping them.

ing with time is less trivial. The "quasi-geostrophic" turbulence introduced by Charney, assuming balanced 'enstrophy', predicts $H = 1$. Fluctuation spectra, especially when considering the structures revealed by different exponents H, provide generally rich and complex insights into self-similar phenomena [cite LS]

Key Outcome: Fluctuation analysis

Fluctuation analysis is focused on the notion that the climate system is noisy. It provides a great way to identify timescales over which negative, stabilising feedbacks dominate from those over which fluctuations accumulate and are possibly amplified by positive feedbacks. It is also linked to methods to characterise the frequency, amplitude and recurrence of extreme events, which can be characteristic of certain kinds of dynamics (turbulence, excitable dynamics).

Further Reading

C. W. Arnscheidt and D. H. Rothman (2022). "Presence or absence of stabilizing Earth system feedbacks on different time scales". In: *Science Advances* 8.46. ISSN: 2375-2548. DOI: 10.1126/sciadv.adc9241. URL: http://dx.doi.org/10.1126/sciadv.adc9241

1.2 Spectral description of variability

Besides fluctuations, another important characteristic of the climate system is the presence of periodic and quasiperiodic patterns. Perhaps the most obvious example is the daily cycle: every day, temperatures are higher near noon than at midnight due to the diurnal cycle of incoming solar radiation. Similarly, temperatures and sometimes precipitation exhibit a clear annual cycle in most parts of the world. These are examples of forced oscillations, which can be explained using a linear energy balance model. More generally, low-order dynamical systems are commonly used to describe specific dynamics of the climate system.

A classic example is the El Niño-Southern Oscillation (ENSO). Here, positive feedback (such as the Bjerknes feedback) combines with delayed responses linked to the propagation of Kelvin waves and Rossby waves to produce an oscillation.

These phenomena involve complex interactions between external forcings (e.g., the annual insolation cycle) and nonlinear internal dynamics, resulting in the quasiperiodic occurrence of El Niño events. Key concepts from nonlinear dynamics such as limit cycles, excitable dynamics, nonlinear resonance, and synchronization, and, of course, transition to chaos, are essential to understanding these phenomena and will be discussed in Chapter 4. On timescales of tens of thousands of years or more, quasiperiodic changes in incoming solar radiation driven by slow variations in Earth's orbital parameters (obliquity, precession, and eccentricity) induce environmental changes visible in geological records. This includes the glacial-interglacial cycles that have characterized the Pleistocene for nearly 3 million years.

Understanding these phenomena requires both physical considerations

(e.g., ice sheet dynamics and the carbon cycle) and nonlinear concepts such as synchronization and nonlinear resonance. In section 1.1.3, we introduced briefly the Lorenz–Saltzman system. It is common to use small models of this type to study different climatic phonemona. For example, in Chapter 6 we will introduce the Winton model of deep-decoupling oscillations, which can be intrepreted as a simple, sketchy interpretation of the cause of temperature and circulation changes observed during past glacial periods. Simple models have also been devised to explain ENSO. The merit of these models is to offer an explanation to recurring or quasi-recurrent dynamics. The common point of these models is that they display characteristic periodic or quasi-periodic pattern which are the signature of an interplay between feedbacks of different strength, or operating at diffrent time scales.

To identify the temporal patterns associated with periodic or quasi-periodic patterns, a power spectrum approach, consisting in projecting the time series onto a basis to identify its main modes, is more adequate.

Classically, and perhaps most naturally, the Fourier basis consisting of sines and cosines of different frequencies come to mind. The power spectrum density of a stationary process $x(t)$ is the square modulus of its Fourier transform, normalised by the observation time:

$$\mathrm{PSD}(f) = \lim_{t\to\infty} \left\| \frac{1}{t} \int_{-\frac{t}{2}}^{+\frac{t}{2}} x(t) e^{-i2\pi f t}\, \mathrm{d}t \right\|^2.$$

Parseval's Theorem (also called Rayleigh's identity) tell us that the integral of the PSD is the total variance of the process, so that the power density can be undertood as a decomposition of the signal energy density accross frequencies. Hence, if a signal contains some periodic pattern of period P, we expect a peak in the density spectrum at $f = 1/P$. From this line of tought comes the idea that climatic precesses will have spectral signatures, that ought to be captured by the models aimed at representing them.

rk on these
ns

- refer to Franzke and Von der Heydts reviews. Show figures and examples.
- quasiperiodic processes: diluted power and may be undistinguishable from the background. Different startegies: ssa, wavelet. Will review wavelet later as specific

- periodogram is an inconsistent estimator of the psd. Hence methods balancing bias and variance, admitting some bias in power but less variance making it a more reliable detector of quasi- or periodic signals. multi-taper

1.3 Fluctuation analysis revisited: Wavelets

Sorry draft notes. This can be a bit technical and has to be developed.
Haar is a particular case of a wavelet decomposition. See Parsival and Walden book + continuous wavelet transform from Mallat.
Back and through between the wavelet (fluctuation) spectra and power density involve the Wiener-Kinchin theorem, according to which the auto-correlation and PSD are Fourier of each other.
The trick is that when computing variance, we have to write a double integral and if the expectation of the signal is zero, then the double integral reduces to an integral over the auto-covariance, which can then be linked to the power spectrum.

1.3.1 Fluctation spectrum is a wavelet specturm

Percival and Walden, p. 15, sect 1.3 "as discussed in chapter 8, an energy decomposition is closely related to the concept of the wavelet variance, which partitions the variance of a process across dyadic scales. The wavelet variance is a succinct alternative to the power spectrum based on the Fourier transform, yielding a scale-based analysis that is often easier to interpret than the frequency-based spectrum."
Percival and Walden p. 266 for Stationary Stochastic processe, p. p. 268 eq 268 for PSD of filtered signal = products of PSD of filter and signal; say also that this is generalisable to non-random signals, given the definition af a Wavelet (his sect. 4.2); 302 eq 302 for correspondance between Wavelet variance and product of PSD of wavelet * signal. p. 305 for interpretation of wavelet spectrum as power spectrum integrated over intervals.
PSD of haar wavelet (attention, omega definition of TF):

$$\hat{H}(\omega) = \frac{i}{\sqrt{2\pi}e^{-i\frac{\omega}{2}}\sin(\omega/4)\,\mathrm{sinc}(\frac{\omega}{4})}, \text{withsinc}(\omega) = \frac{\sin(\omega)}{\omega}. \tag{1.2}$$

and successive transforms, of inceasingly *smaller* scales, obtained by multipling ω by 2^j.
See also Walden for zero padding and circular shift for assessing the wavelet variance (he calls it the MODWT).

1.3.2 Link between fluctuation and power spectrum

Here is a heuristic argument linking the fluctuation spectrum to the power spectral density. It implicitly assumes that the time series has a power-law fluctuation spectrum and takes for granted that the power spectral density is also scaling.
Assume, thus,

$$\left\langle \big(x(t+\delta t) - x(t)\big)^2 \right\rangle \sim \delta t^{2H}$$

This variance associated with fluctations that are δt apart is, roughly speaking, the total variance of the system, but filtering only for frequencies $\omega < 1/\Delta t$.
Hence:

$$\delta t^{2H} \sim \int_0^{\omega} \mathrm{PSD}(\omega')\mathrm{d}\omega' \sim \int_0^{\omega} (\omega')^{-\beta}\mathrm{d}\omega' \sim \omega^{-\beta+1} \sim \delta t^{+\beta-1}$$

This produces the scaling relationship

$$\boxed{2H = \beta - 1 \Leftrightarrow 2H + 1 = \beta} \tag{1.3}$$

We can verify the relationship with a few sanity checks:

- Decorrelated, random noise has a flat power specturm ($\beta = 0$) but scaling fluctations decaying with scale, $\left\langle \big(x(t+\delta t) - x(t)\big)^2 \right\rangle \sim -1$, that is, $H = -1/2$.

- The randow walk has a power density specturm with slope 2 ($\beta = -2$) (infinite variance; this is not a stationary time series), and scaling fluctations increasing with scale, $H = 1/2$.

work on the following items

- compare fluctuation and density power spectrum of orstein uhlenbeck process
- attention la psd du orstein uhlenbeck se calcule souvent en fonction de ω pas de f. Spectre OU $\propto \frac{k^2}{k^2+\omega^2}$ avec $k = 1/\tau$. Tend vers 1 pour $\omega = 0$. Mais du coup $\omega = 2\pi f$ ce qui explique le facteur 2π dans la correspondance Haar / PSD.
- to do : introduce to multi-fractal processes.

1.4 Sythesis: what are climate regimes?

Answer: Consistent model assumptions

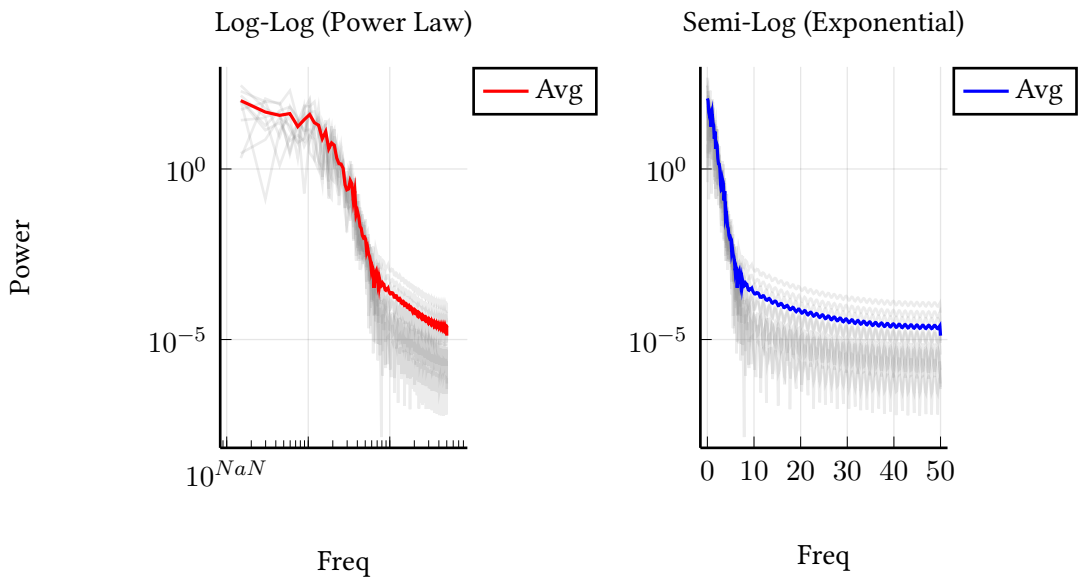

Figure 1.4: to be further commented on. This is the periodogram of the Lorenz 63 model.

Chapter 2

Stochastic EBMs

2.1 1-D EBM

Consider a one-box ocean, submitted to heat exchange at the top. Call S its area, z its depth, ρ its density, C_p the caloric capacity of water, and net F^n the net flux of energy per unit area, we have:

$$\rho z S C_p \frac{\mathrm{d}T}{\mathrm{d}t} = F^n \tag{2.1}$$

We now assume that the net flux is the difference between an *incoming* flux F, and a response, outgoing flux aT. It is further perturbed by a zero-average, white noise of intensity σ caused by atmospheric fluctuations: $F^n = F - aT + \sigma\dot{W}$. We also note $C = \rho z C_p$.

$$C\frac{\mathrm{d}T}{\mathrm{d}t} = F - aT + \sigma\dot{W} \tag{2.2}$$

This is an informal shortcut for the more properly written stochastic differential equation $C\,\mathrm{d}T = (F - aT)\,\mathrm{d}T + \sigma\,\mathrm{d}W$.
Taking the Fourier transform (denoted $\hat{T}(\omega)$) on both sides, we find (Fourier transform of constant is zero almost everywhere, except in zero)

$$Ci\omega\hat{T} = -a\hat{T} + \sigma\hat{\dot{W}}, \tag{2.3}$$

that is:

$$\hat{T} = \frac{\sigma\hat{\dot{W}}}{a/C + i\omega} \tag{2.4}$$

The power spectrum is the square modulus of the Fourier transform. Using $\mathbb{E}(||\hat{\dot{W}}||^2) = 1$ (the expected power spectrum of white noise is flat), we find:

$$\text{PSD}(\omega) = \frac{\sigma^2}{a^2/C^2 + \omega^2} \tag{2.5}$$

This is a Lorenzian, characterized by slope -2 at high frequency, and 0 at low frequency. The turning point is $\omega = a/C$, that is, the characteristic time $\tau_c = 1/f_c = 1/(2\pi\omega_c) = C/(2\pi a)$.

2.2 2-D EBM

Consider two communicating boxes, with temperatures T_1 (upper box) and T_2 (lower box), exchanging a flux per unit area $k(T_1 - T_2)$, from the upper box to the lower one. The upper box, as in the former section, exchanges aT_1 with the atmosphere and is also submitted to stochastic forcing. We have this time a system of two coupled stochastic differential equations:

$$C_1 \frac{\mathrm{d}T_1}{\mathrm{d}t} = -(a+k)T_1 + kT_2 + F - \sigma\dot{W} \tag{2.6}$$

$$C_2 \frac{\mathrm{d}T_2}{\mathrm{d}t} = kT_1 - kT_2 \tag{2.7}$$

The system may be rewritten in matrix form, using $\boldsymbol{T} = (T_1, T_2)$, $\boldsymbol{F} = (F, 0)$ and $\dot{\boldsymbol{W}} = (\dot{W}_1, \dot{W}_2)$ (i.e., we generalize and assume a multidimensional noise vector):

$$\frac{\mathrm{d}\boldsymbol{T}}{\mathrm{d}t} = A\boldsymbol{T} + \frac{\boldsymbol{F}}{C_1} + B\dot{\boldsymbol{W}}, \tag{2.8}$$

where A and B are matrices defined as:

$$A = \begin{pmatrix} -(a+k)/C_1 & k/C_1 \\ k/C_2 & -k/C_2 \end{pmatrix} \quad B = \begin{pmatrix} \sigma/C_1 & 0 \\ 0 & 0 \end{pmatrix}$$

An efficient way to find the power spectrum is merly to isolate T as we did in the 1-D EBM, using that $\frac{\mathrm{d}\hat{\boldsymbol{T}}}{\mathrm{d}t} = i\omega I\boldsymbol{T}$, with I the identity matrix, and that the expected power spectrum of white noise is flat:

$$\hat{\boldsymbol{T}} = -(A - i\omega I)^{-1}B\hat{\boldsymbol{W}}$$

The power spectrum is $\hat{\boldsymbol{T}}\hat{\boldsymbol{T}}^\dagger$. The † is the symbol for the adjoint, that is, the complex conjugate transpose. It is a slight abuse of notation for vectors, but the meaning is that if $\boldsymbol{T}$ is a column vector, then $\boldsymbol{T}^\dagger$ is a line vector, and $\hat{\boldsymbol{T}}\hat{\boldsymbol{T}}^\dagger$ is an outer product. The result is a matrix, whose diagonal elements are the power spectra of the two components of $\boldsymbol{T}$, and off-diagonal, cross-spectra.
With this notation, and using again that the expected power spectrum of white noise is flat (that is: $\mathbb{E}(\dot{\boldsymbol{W}}\dot{\boldsymbol{W}}^\dagger) = I$),

$$\mathrm{PSD}(\boldsymbol{T}) = (A - i\omega I)^{-1}BB^\dagger((A - i\omega I)^{-1})^\dagger$$

In this particular problem, $BB^\dagger$ is a matrix whose only the first element is non-zero. It is $b^2 \stackrel{\text{def}}{=} \sigma^2/C_1^2$. In this praticular configuration, if we call

$$L = (A - i\omega I)^{-1} = \begin{pmatrix} l_{11} & l_{12} \\ l_{21} & l_{22} \end{pmatrix}$$

one finds that the $\mathrm{PSD}(T_1) = b^2|l_{11}|^2$ and $\mathrm{PSD}(T_2) = b^2 l_{21}l_{21}^\star$.
We are almost done. In this reasonably simple problem, all what we need to do is to invert a 2×2 matrix. We know its form:

$$\frac{1}{\det(A - i\omega I)} \begin{pmatrix} A_{22} - i\omega & -A_{12} \\ -A_{21} & A_{11} - i\omega \end{pmatrix}$$

Now, observe that $\det(A - i\omega)$ is the characteristic polynomial of A; this is, it must be equal to $(\lambda_1 - i\omega)(\lambda_2 - i\omega)$ where $\lambda_{1,2}$ are the eigenvalues of A. We are nearly there:

$$\text{PSD}(T_1) = \frac{b^2(A_{22}^2 + \omega^2)}{(\lambda_1^2 + \omega^2)(\lambda_2^2 + \omega^2)}$$
$$\text{PSD}(T_2) = \frac{A_{21}^2}{(\lambda_1^2 + \omega^2)(\lambda_2^2 + \omega^2)}$$

It is possible to re-express these spectra as a sum of Lorenzians. Take, for example:

$$\frac{A_{22}^2 + \omega^2}{(\lambda_1^2 + \omega^2)(\lambda_2^2 + \omega^2)} = \frac{\alpha}{\lambda_1^2 + \omega^2} + \frac{\beta}{\lambda_2^2 + \omega^2} \tag{2.9}$$

α and β can be found by matching coefficients.

Key Outcome: Power spectrum of linear box model

The power spectrum of this linear two box model is the superposition of two Lorentzians, with characteristic frequencies related to the two eignevalues of the transfer matrix : it reflects the two characteristic time of this system with two degrees of freedom. This result can be also understood as consistent with the principle of mode-decomposition of a linear system: two 2-dimensional system can be projected on two decoupled systems governed by the eigenvalues of A.

Analytical spectrum of two-box model

Compute (without simulations) the power spectrum of T_1 and T_2. Assume (and justify) $a = 1.25$ W/m^2, $a/C1 = k/C1 = 1/(5\text{years})$ and $k/C_2 = 1/(500$ years). You can solve the eigenvalue problem using a computer language, e.g. Python, Julia or R.

Next one can simulate the process, using numerical integration. The receipt, for a stochastic differential equation of the type $\mathrm{d}T = aT + \sigma\,\mathrm{d}W$, according to the Euler Maruakama scheme with a time step k:

$$T_{i+1} = T_i + a\delta t T_i + \sqrt{\delta t}\sigma n_i, \tag{2.10}$$

where n_i is a random number drawn from a Normal distribution ($\mathcal{N}(0,1)$). From there, its power specturm can be estimated from a periodogram. Standard routines exist and are easily found for mainstream languages. It can also easily obtained from the discrete Fourier transform, computed with the Fast fourier transform. Take $\mathbf{i} = [0 \dots N-1]$ the index (N elements), $t = [0, k \dots (N-1)] = \mathbf{i}k$ the vector of times, and $\omega = [0, \frac{2\pi}{Nk} \dots 2\pi\frac{N-1}{Nk}] = 2\pi\frac{\mathbf{i}}{Nk}$. Then the periodogram of T is

$$p(\omega) = ||2\delta t \frac{\text{FFT(T)}}{N}||^2, \text{for} \omega \in [0, \pi/k[. \tag{2.11}$$

The periodogram $p(\omega)$ is unbiased but inconsistent estimator of the PSD. Its variance grows towards infinity at low frequencies. There are better estimators, though for numerical simulations it sufficies to produce several simulations (typically, one hundred) and average the corresponding periodograms.

Numerical computation of power density spectrum

Reconsider the two box model; produce numerical simulations and estimate, numerically, the spectrum. Does it match the analytical solution ?

Key Outcome: Towards long-memory spectrum

Now we can predict that a system with N boxes, communicating pairwaise, will be characterised by a tri-diagonal A. Tridiagonal matrices are characterised by a specturm of eigenvalues. Typically, for a tridiagonal $(k, -2k, k)$ the spectrum of eigenvalues is $\lambda_j = -4k \sin^2((j\pi)/2(n+1))$, for n boxes. Thus we have an almost continum set of eigenvalues spanning the whole range of time scales. At the limite of great n, the power spectrum will converge to a function proportional to ω^{-1} (no more distinction between the Brownian (drifting) regime and the white noise regime).

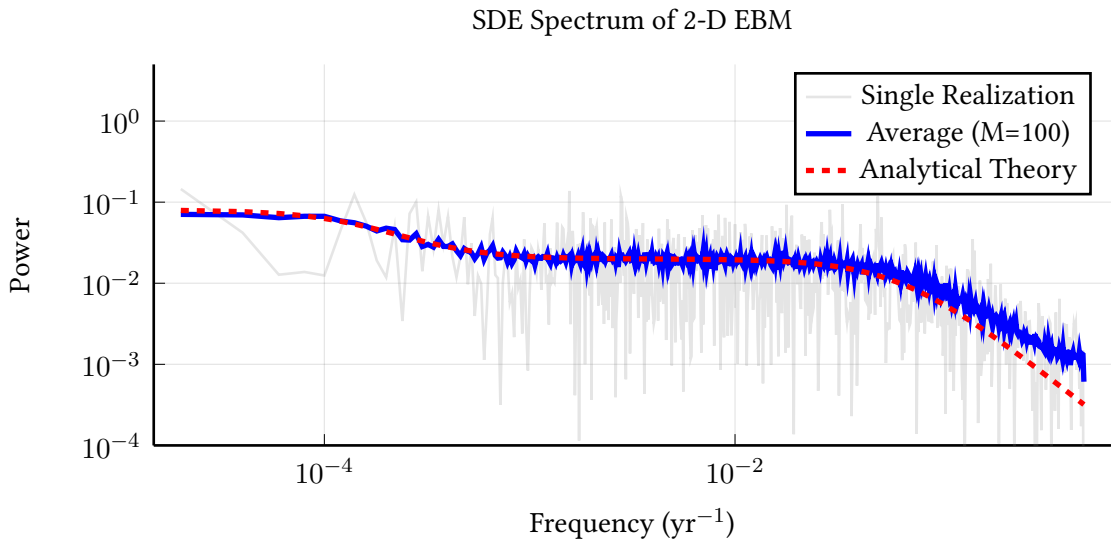
SDE Spectrum of 2-D EBM
Single Realization
Average (M=100)
Analytical Theory
Power
10^{0}
10^{-1}
10^{-2}
10^{-3}
10^{-4}
10^{-4}
10^{-2}
Frequency (yr^{-1})

Chapter 3

Linear waves

3.1 Basic notions

3.1.1 Stability

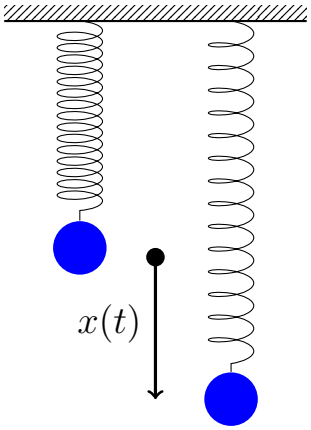

The movement of a mass m attached to a spring of tension parameter k is

$$m\ddot{x} = -kx.$$

It admits as general solution

$$x(t) = Ae^{\lambda t} + Be^{-\lambda t}$$

where $\lambda = \sqrt{-k/m} = i\sqrt{k/m}$.

Having λ fully imaginary means that the solution oscillates at constant amplitude.

The imaginary part is interpreted as an angular velocity.

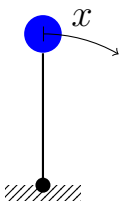

In the upside pendulum (length L), the equation around the unstable equilibrium is:

$$\ddot{x} = \frac{g}{L}x + \mathcal{O}(x^2).$$

The linearised equation is thus:

$$\ddot{x} = \frac{g}{L}x.$$

It admits as general solution

$$x(t) = Ae^{\lambda t} + Be^{-\lambda t},$$

where $\lambda = \sqrt{\frac{g}{L}}$. The units of λ are s^{-1}. Unless initial conditions are delicately chosen such as to neutralise A, the unstable solution will generally dominate.

3.1.2 Wave equation

In mathematical physics, the wave equation is defined as:

$$\frac{\partial^2 u}{\partial t^2} = c^2 \frac{\partial^2 u}{\partial x^2}.$$

It can be solved in different ways.
One approach is to impose a *progressive wave* of the form

$$u(x,t) = Ae^{i(kx-\omega t)}.$$

Substitution gives the *dispersion relationship* $\omega = \pm kc$.

The phase velocity c_ϕ, defined as $c_\phi = \omega/k$, is constant. Hence, the *general solution* is:

$$u(x,t) = \sum_j A_j e^{ik_j(x-ct)} + \sum_j B_j e^{ik_j(x+ct)}$$

The A_j and B_j are set by the initial conditions on u and $\frac{\partial u}{\partial t}$ at $t = 0$.
Another approach is to observe the following factorisation:

$$\begin{aligned} (\frac{\partial^2}{\partial t^2} - c^2 \frac{\partial^2}{\partial x^2})u &= 0, \\ (\frac{\partial}{\partial t} + c\frac{\partial}{\partial x})(\frac{\partial}{\partial t} - c\frac{\partial}{\partial x})u &= 0. \end{aligned}$$

At this point, a well-known trick is to impose a change of variable. Indeed, pose:

$\begin{cases} r = x - ct \\ s = x + ct \end{cases}$, equivalent to $\begin{cases} 2x = r + s \\ 2ct = r - s \end{cases}$, gives:

$$\begin{aligned} \frac{\partial u}{\partial r} &= \frac{\partial u}{\partial t}\frac{\partial t}{\partial r} + \frac{\partial u}{\partial x}\frac{\partial x}{\partial r} = \frac{1}{2c}(\frac{\partial}{\partial t} + c\frac{\partial}{\partial x})u \\ \frac{\partial u}{\partial s} &= \frac{\partial u}{\partial t}\frac{\partial t}{\partial s} + \frac{\partial u}{\partial x}\frac{\partial x}{\partial s} = -\frac{1}{2c}(\frac{\partial}{\partial t} - c\frac{\partial}{\partial x})u \end{aligned}$$

It has for general solution

$$u(x,t) = F(r(x,t)) + G(s(x,t)) = F(x - ct) + G(x + ct).$$

The curves of constant r and s are called characteristics. The flow is constant along them (as long as F and G are compact enough).

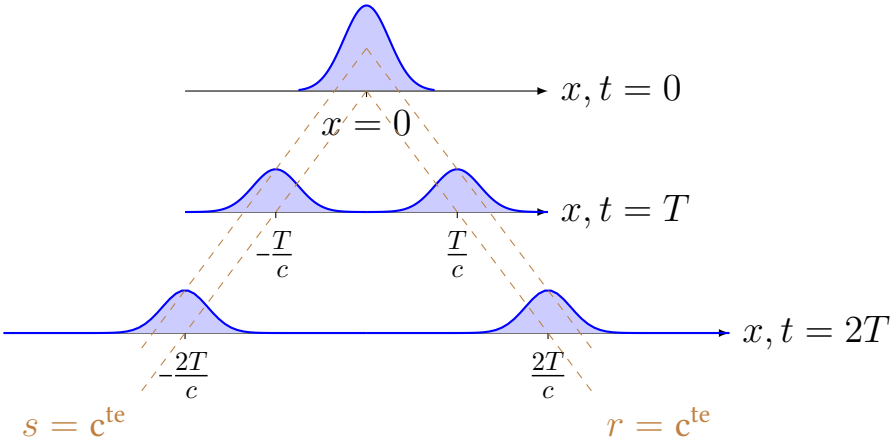

3.1.3 Basic hydrodynamic equations

3.1.3.1 Euler equation

On a rotating frame with angular velocity $\boldsymbol{\Omega}$, the Euler equation reads:

$$\frac{\partial \boldsymbol{u}}{\partial t} + \boldsymbol{u} \cdot \nabla \boldsymbol{u} + 2\Omega \times \boldsymbol{u} = -\frac{\boldsymbol{\nabla} p}{\rho} - \boldsymbol{\nabla}\Phi, \qquad \text{(Euler)}$$

where p is pressure, ρ, density, Φ potential or geopotential and $\boldsymbol{u}$, velocity. As $\boldsymbol{\nabla} u^2 = 2(\boldsymbol{u} \cdot \nabla \boldsymbol{u} + \boldsymbol{u} \times \underbrace{(\boldsymbol{\nabla} \times \boldsymbol{u})}_{\boldsymbol{\zeta}})$, (Euler) becomes:

$$\frac{\partial \boldsymbol{u}}{\partial t} + \boldsymbol{\nabla}\frac{u^2}{2} + \underbrace{(\boldsymbol{\zeta}_p + \boldsymbol{\zeta})}_{\zeta_a} \times \boldsymbol{u} = -\frac{\boldsymbol{\nabla} p}{\rho} - \boldsymbol{\nabla}\Phi,$$

$\boldsymbol{\zeta}_p = 2\boldsymbol{\Omega}$ is the planetary vorticity, and $\boldsymbol{\zeta}_a$, the absolute.

3.1.3.2 Incompressible flow approximation

The incompressible flow approximation consists in neglecting the variations of density in the continuity equation. The flow is then effectively incompressible. It is generally valid when the flow velocity is well below the speed of sound.
This is one element of the Boussinesq approximation.

$$\boldsymbol{\nabla} \cdot \boldsymbol{u} = 0 \qquad \text{(Boussinesq)}$$

3.1.3.3 Vorticity equation (in the Boussinesq approximation)

We make use of the generic formula

$$\boldsymbol{\nabla} \times (\boldsymbol{a} \times \boldsymbol{b}) = \boldsymbol{a}(\boldsymbol{\nabla} \cdot \boldsymbol{b}) - \boldsymbol{b}(\boldsymbol{\nabla} \cdot \boldsymbol{a}) + (\boldsymbol{b} \cdot \boldsymbol{\nabla})\boldsymbol{a} - (\boldsymbol{a} \cdot \boldsymbol{\nabla})\boldsymbol{b},$$

using $\boldsymbol{\nabla} \cdot \boldsymbol{u} = 0$ (Boussinesq), this gives us:

$$\boldsymbol{\nabla} \times (\boldsymbol{\zeta}_a \times \boldsymbol{u}) = \boldsymbol{u} \cdot \nabla \boldsymbol{\zeta}_a - \boldsymbol{\zeta}_a \cdot \boldsymbol{\nabla} \boldsymbol{u}$$

Taking the $\boldsymbol{\nabla}\times$ of (Euler), and using $\boldsymbol{\nabla} \times \boldsymbol{\nabla} \boldsymbol{a} = 0$:

$$\underbrace{\frac{\partial \boldsymbol{\zeta}_a}{\partial t} + \boldsymbol{u} \cdot \nabla \boldsymbol{\zeta}_a}_{\frac{\mathrm{D}\boldsymbol{\zeta}_a}{\mathrm{D}t}} - \boldsymbol{\zeta}_a \cdot \boldsymbol{\nabla} \boldsymbol{u} = \boldsymbol{\nabla} p \times \boldsymbol{\nabla} \left(\frac{1}{\rho} \right).$$

The $\boldsymbol{\zeta}_a \cdot \boldsymbol{\nabla} \boldsymbol{u}$ is not quite trivial to understand: this is a vector with three components: $\boldsymbol{\zeta}_a \cdot \nabla u$, $\boldsymbol{\zeta}_a \cdot \nabla v$, and $\boldsymbol{\zeta}_a \cdot \nabla w$. It measures the shear of velocity along the vorticy vector.
We get that vorticity can be created by

- Stretching.
- A baroclinic torque,

An irrotational barotropic fluid, with no (or negligible) planetary vorticity, remains irrotational.

Small scale, irrotational (thus, laminar) flows, with no friction (Euler equation), remain irrotationnal.

3.1.3.4 Bernoulli principle

In a *barotropic* fluid, $\rho = \rho(p)$. This implies that $\frac{\boldsymbol{\nabla} p}{\rho}$ can be re-expressed as a gradient:

$$\frac{\boldsymbol{\nabla} p}{\rho} = \boldsymbol{\nabla} \int_{p_0}^{p} \frac{\mathrm{d}p}{\rho(p)} \overset{\text{def}}{=} \frac{\boldsymbol{\nabla} p^\star}{\rho_0}.$$

We will usually omit the * and the $_0$ and consider that a barotropic flow is a constant-ρ flow.

This implies that in a *barotropic, non-rotational* fluid:

$$-\nabla\left(\frac{u^2}{2} + \frac{p}{\rho} + \Phi\right) = \frac{\partial \boldsymbol{u}}{\partial t}. \qquad \text{(Bernoulli)}$$

This is the time-dependent Bernoulli equation. In the stationary flow (no-time dependence), the term under the gradient is constant in space.

3.1.4 Shallow-water model

We define the shallow-water model (Saint-Venant) as a barotropic, free-surface layer of height $h(x, y, t)$, where *pressure* satisfies the *hydrostatic* approximation (no vertical acceleration). The horizontal velocity $\boldsymbol{u}_h$ is vertically homogeneous (no vertical shear)

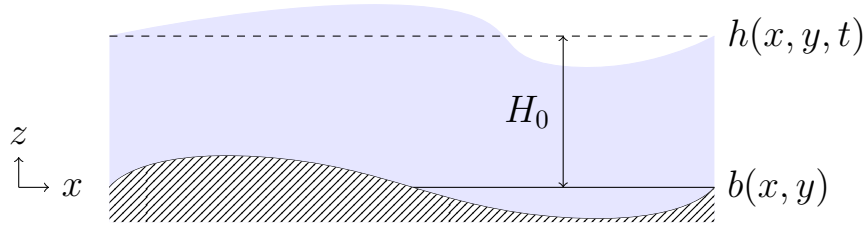

We therefore have $\boldsymbol{u}_h = \boldsymbol{u}_h(x, y, t)$.
The upper boundary condition is $w_u = \frac{\mathrm{D}h(x,y,t)}{\mathrm{D}t}$.
Likewise, $w_b = \frac{\mathrm{D}b(x,y)}{\mathrm{D}t} = \boldsymbol{u}_h \cdot \nabla_h b$.
Integrating (Boussinesq) along the vertical,

$$H \nabla_h \cdot \boldsymbol{u}_h = -\int_b^h w \, \mathrm{d}z = -(w_u - w_b) = -\frac{\mathrm{D}(h-b)}{\mathrm{D}t} \overset{\text{def}}{=} -\frac{\mathrm{D}H}{\mathrm{D}t}.$$

(SV-Hydro.1)

The hydrostatic assumption implies $\boldsymbol{\nabla} p = g \boldsymbol{\nabla} h$.
We speak of *quasi-hydrostratic* flow in the sense that pressure and height are diagnostically linked by the hydrostatic approximation. Thus, from this point of view, there could not be any vertical acceleration. Yet, we admit changes in vertical convergence, thus, changes in vertical velocity when the convergence of the continuity equation, from the continuity equation.
The vertically-integrated, horizontal component of the Euler equation then becomes:

$$\frac{\partial \boldsymbol{u}_h}{\partial t} + \boldsymbol{u}_h \cdot \nabla_h \boldsymbol{u}_h + f \boldsymbol{e}_z \times \boldsymbol{u}_h = -g \nabla h, \tag{SV-Hydro.2}$$

where the Coriolis factor $f = 2\boldsymbol{\Omega} \cdot \boldsymbol{e}_z$.

3.2 Gravity waves

3.2.1 Shallow-water gravity waves

This is the simplest case that allows us to illustrate the linear-wave derivation process. Consider the Saint-Venant model, and neglect rotation (large Rossby number):

$$H_0 \nabla \cdot \mathbf{u}_h = -\frac{\partial h}{\partial t},$$
$$\frac{\partial \mathbf{u}_h}{\partial t} = -g \nabla h.$$

Adopt the linear-wave approximation. That is: first determine a reference *steady* state. Here, we take $(\bar{H}, \bar{\mathbf{u}}_h) = (H_0, \mathbf{0})$. Then define anomalies as $(h, \mathbf{u}_h)$. Neglecting all terms of order 2 and above, we obtain the linearized system:

$$H_0 \nabla \cdot \mathbf{u}_h = -\frac{\partial h}{\partial t} \quad \text{and} \quad \frac{\partial \mathbf{u}_h}{\partial t} = -g \nabla h.$$

Taking the time derivative of the first equation and the divergence of the second allows them to combine into the wave equation:

$$\frac{\partial^2 h}{\partial t^2} = g H_0 \nabla^2 h. \tag{3.1}$$

This equation admits a general solution in the form of a complex wave (where $\mathbf{u}_h = (u, v)$):

$$u(x, y, t) = \hat{u}_{kl} e^{i(kx + ly - \omega t)}$$
$$v(x, y, t) = \hat{v}_{kl} e^{i(kx + ly - \omega t)}$$
$$h(x, y, t) = \hat{h}_{kl} e^{i(kx + ly - \omega t)}$$

The relationship between ω and (k, l) is the dispersion relation:

$$\omega^2 = c_g^2 (k^2 + l^2), \quad \text{with } c_g^2 = g H_0. \tag{3.2}$$

The momentum equation links the velocity amplitudes with the height amplitude:

$$\hat{u}_{kl} = \frac{gk}{\omega} \hat{h}_{kl} \quad \text{and} \quad \hat{v}_{kl} = \frac{gl}{\omega} \hat{h}_{kl}.$$

3.2.2 Setting initial conditions

Setting $\hat{u}_{kl}$ from initial conditions requires a detour through the formalism of Fourier transforms. The physical field $u(x, y, t)$ is understood to be the real part of an inverse Fourier transform, which synthesizes all modes.

$$u_{\text{phys}}(x, y, t) = \text{Re}\left[\frac{1}{(2\pi)^2}\iint \hat{u}_{kl} e^{i(kx+ly-\omega t)}\,\mathrm{d}k\,\mathrm{d}l\right]. \tag{3.3}$$

Expanding the real part using $\text{Re}(z) = \frac{1}{2}(z+z^*)$, we see that at each mode, the real field is a combination of forward ($-\omega t$) and backward ($+\omega t$) propagating components. To recover the complex amplitude $\hat{u}_{kl}$ from observed fields at $t = 0$, we use both the field u_{phys} and its time derivative.
Taking the Fourier transform $\mathcal{F}\{f\} = \iint f(x, y)e^{-i(kx+ly)}\,\mathrm{d}x\,\mathrm{d}y$ of the physical observations at $t = 0$:

$$\mathcal{F}\{u_{\text{phys}}\} = \frac{1}{2}(\hat{u}_{kl} + \hat{u}^*_{-k,-l})$$
$$\mathcal{F}\left\{\frac{\partial u_{\text{phys}}}{\partial t}\right\} = \frac{-i\omega}{2}(\hat{u}_{kl} - \hat{u}^*_{-k,-l})$$

We can then isolate the complex amplitude:

$$\hat{u}_{kl} = \mathcal{F}\{u_{\text{phys}}\}(k, l) + \frac{i}{\omega}\mathcal{F}\left\{\frac{\partial u_{\text{phys}}}{\partial t}\right\}(k, l).$$

The real part of $\hat{u}_{kl}$ is provided by the instantaneous spatial distribution of the field, while its imaginary part is recovered from its trend (time derivative). The angular velocity ω is set by the dispersion relationship. This process ensures that the initialized complex field correctly captures the phase and direction of the wave propagation, for any smooth initial condition.

3.2.3 Capillary waves

At short wavelengths, capillary effects dominate. We maintain the shallow-water formalism, but capillary effects are accounted for with an additional (negative) pressure term in the Bernoulli equation:

$$p = p_0 - T\frac{\partial^2 h}{\partial x^2}$$

The surface boundary condition becomes

$$\frac{\partial \varphi}{\partial t} + gh - \frac{T}{\rho}\frac{\partial^2 h}{\partial x^2} = 0,$$

and, after calculation, one finds:

$$c^2 = \left(\frac{g}{k} + \frac{Tk}{\rho}\right).$$

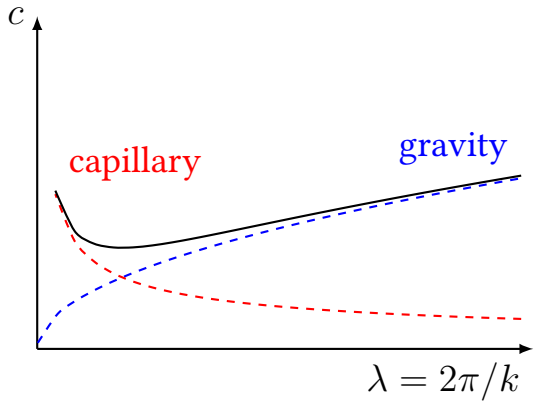

For typical values of T ($71 \cdot 10^{-3}$ N/m), one finds that the typical scale of capillary waves is centimetric.

3.2.4 Deep-water, barotropic, non-rotational gravity waves

We leave the horizontal plane and the shallow-water equations, and consider the problem along the vertical. We thus address the problem in a 2-D (horizontal-vertical) section, with a velocity $\mathbf{u} = (u, w)$. For deep-water, we need to give up the shallow-water approximation, but restrict the analysis to barotropic, non-rotational flow (we assume the conditions of the Bernoulli flow). Non-rotation is imposed by requiring velocity to derive from a velocity potential φ: $(u, w) = \boldsymbol{\nabla}\varphi$. The flow non-divergence then implies $\nabla^2\varphi = 0$. This is a well-known problem in mathematical physics: solving the Laplace equation. If we assume progressive waves in the horizontal plane, then the solution

$$\varphi = e^{i(kx-\omega t)}(\hat{\varphi}^+ e^{kz} + \hat{\varphi}^- e^{-kz})$$

guarantees the non-divergence solution. We now need to specify boundary conditions which will determine the $\varphi^{\pm}$. Set the reference surface as $z = 0$, and linearize (neglect advection terms), and define the height anomaly h above the reference surface.

$$\frac{\partial h}{\partial t}(x, y, t) = w|_{z=0} = \left.\frac{\partial \varphi}{\partial z}\right|_{z=0}.$$

If the water is deep, $\hat{\varphi}^-$ must be zero. Consider this case. To connect h with φ we need the time-dependent Bernoulli equation

$$\boldsymbol{\nabla}\left(\frac{\partial\varphi}{\partial t}+\frac{u^2}{2}+\frac{w^2}{2}+\frac{p}{\rho}+\Phi\right)=0.$$

What is in the gradient can in fact be any function of time (but constant in space), which we can choose at our convenience. We get a boundary condition for ϕ by imposing the term under the gradient to be equal to 0 at $z=0$ (we can use a hydrostatic approximation to get the pressure at $z=0$):

$$\frac{\partial\varphi}{\partial t}+gh=0,\ \text{at } z=0\Rightarrow\frac{\partial^2\varphi}{\partial t^2}=-g\frac{\partial\varphi}{\partial z}.$$

We may now substitute the solution to obtain $\boxed{\omega=\pm\sqrt{gk}}$. This is our dispersion relation. The phase velocity $c_p=\sqrt{\frac{g}{k}}$, and the group velocity $c_{\text{group}}=\sqrt{\frac{g}{2k}}$. If we had a finite depth at, say, $z=-H$, we would have a no-flux boundary condition:

$$0=w|_{z=-H}=\left.\frac{\partial\varphi}{\partial z}\right|_{z=-H}=e^{i(kx-\omega t)}k(\hat{\varphi}^+e^{kH}-\varphi^-e^{-kH})$$

which is satisfied for $\varphi^-=e^{-2kH}\hat{\varphi}^+$. This implies (after calculations) that the amplitude of these surface gravity waves grows from the bottom to the surface as $\sinh(k(H+z))$.

One obtains in this case

$$\boxed{c_p^2=\frac{g}{k}\tanh(kH)}.$$

At the limit of small H we recover the shallow-water relationship.

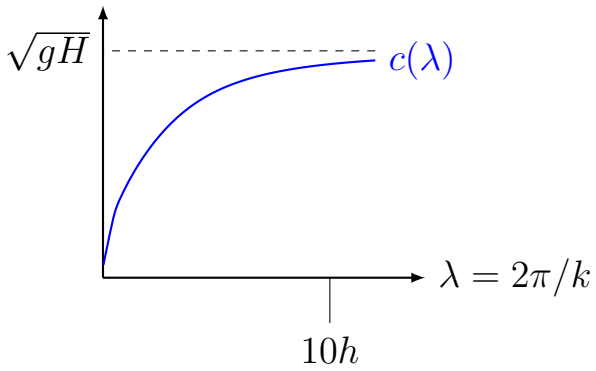

3.2.5 Internal gravity waves

The waves in the previous sections are generated by the movement of the free surface. We are now interested in non-barotropic waves that are generated by the density gradient along the vertical, and which may travel upwards or downwards. These are the internal gravity waves. We keep the Boussinesq approximation but no longer use the hydrostatic approximation. The full system is thus the Euler equation along with the state equation for density, but still assuming a non-divergent flow, in the (x, z) plane:

$$\begin{aligned}\rho\left[\frac{\partial \mathbf{u}}{\partial t} + \boldsymbol{u}\cdot\nabla\mathbf{u}\right] &= -\boldsymbol{\nabla} p + \rho\boldsymbol{g},\\ \boldsymbol{\nabla}\cdot\mathbf{u} &= 0,\\ \frac{\partial \rho}{\partial t} + \boldsymbol{u}\cdot\nabla\rho &= 0.\end{aligned}$$

We linearize around a reference state $p_r(z)$, $\rho_r(z)$, and $\mathbf{u}_r = \mathbf{0}$: giving

$$\begin{aligned}\rho_r\frac{\partial \tilde{u}}{\partial t} &= -\frac{\partial \tilde{p}}{\partial x}, & \rho_r\frac{\partial \tilde{w}}{\partial t} &= -\frac{\partial \tilde{p}}{\partial z} - \tilde{\rho}g,\\ \frac{\partial \tilde{u}}{\partial x} + \frac{\partial \tilde{w}}{\partial z} &= 0, & \frac{\partial \tilde{\rho}}{\partial t} + \tilde{w}\frac{\mathrm{d}\rho_r}{\mathrm{d}z} &= 0.\end{aligned}$$

We search for solutions of the kind $\tilde{u} = \hat{u}(z)e^{i(kx-\omega t)}$. After calculation and simplification, this generates an equation of the form:

$$\tilde{u}'' + \frac{{\rho_r}'}{\rho_r}\tilde{u}' + k^2\left(\frac{N^2}{\omega^2} - 1\right)\tilde{u} = 0,$$

where the *buoyancy frequency* (also called Brunt-Väisälä frequency) $N \overset{\text{def}}{=} -\frac{g}{\rho_r}\frac{\mathrm{d}\rho_r}{\mathrm{d}z}$ and the prime is a z-derivative. If we further adopt the assumption of a profile $\rho_r(z) \propto e^{-z/H}$ such that $\frac{\mathrm{d}\rho_r}{\mathrm{d}z} = -\frac{\rho_r}{H}$, we have, after further calculations:

$$\tilde{w} \propto e^{-z/2H}e^{i(kx+lz-\omega t)}, \quad \text{where } \omega^2 = \frac{N^2k^2}{\left(k^2 + l^2 + \frac{1}{4H^2}\right)}.$$

Consider, for illustration, the limit of large H ($1/H \to 0$), we obtain, after calculation:

$$\boldsymbol{c}_g = \frac{\omega l}{(k^2 + l^2)}(l, -k)$$

The wave packets travel in a direction which is orthogonal to the crests!

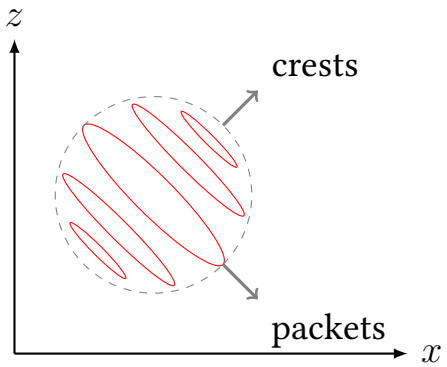

Internal gravity waves play an important role in vertical mixing. They may be excited by orography, and, in the atmosphere, grow with altitude due to the decrease in density.

3.2.6 Accounting for stratification in a two-layer Saint-Venant model

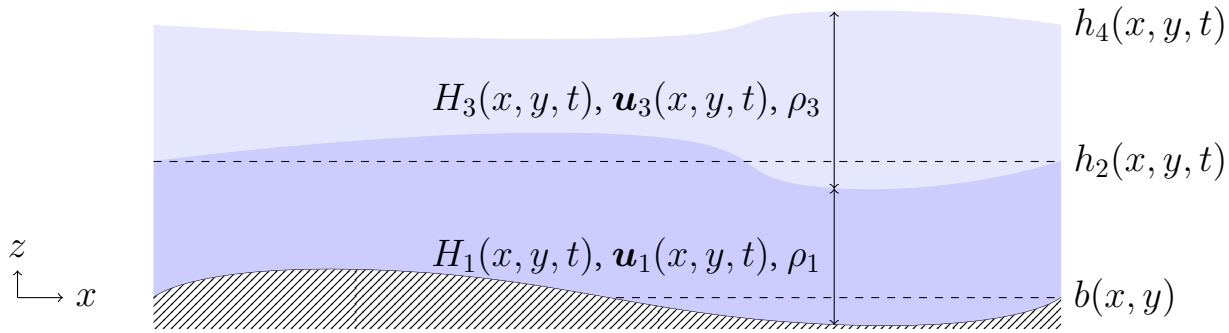

Continuity
(**u** is here horizontal velocity):

$$H_{1,3}\boldsymbol{\nabla}\cdot\mathbf{u}_{1,3} = -\frac{\mathrm{D}H_{1,3}}{\mathrm{D}t}$$

Momentum:

$$\frac{1}{\rho_3}\frac{\mathrm{D}u_3}{\mathrm{D}t} = -g\frac{\boldsymbol{\nabla}h_4}{\rho_3}$$

$$\frac{1}{\rho_1}\frac{\mathrm{D}u_1}{\mathrm{D}t} = -g\frac{\rho_3\boldsymbol{\nabla}(h_4 - h_2) + \rho_1\boldsymbol{\nabla}h_2}{\rho_1}$$

We try a solution of the kind $\tilde{h}_{2,4} = \hat{h}_{2,4}e^{i(kx-\omega t)}$. After linearizing and substituting, we find a system of four algebraic equations (consider again

a movement along x only):

$$\left.\begin{aligned} H_{r3}\hat{u}_3 &= c(\hat{h}_4 - \hat{h}_2) \\ H_{r1}\hat{u}_1 &= c\hat{h}_2 \\ c\hat{u}_3 &= g\hat{h}_4 \\ c\hat{u}_1 &= g\left(\frac{\rho_3}{\rho_1}\hat{h}_4 + \hat{h}_2\right) \end{aligned}\right\} \Rightarrow \begin{cases} c^2(\hat{h}_4 - \hat{h}_2) = gH_{r3}\hat{h}_4 \\ c^2\hat{h}_2 = gH_{r1}\left(\frac{\rho_3}{\rho_1}(\hat{h}_4 - \hat{h}_2) + \hat{h}_2\right) \end{cases}$$

(TwoLayerSV)

If $\rho_3 = \rho_1$ we may simply sum up the two equations and recover $c^2 = g(H_{r1} + H_{r3})$. Otherwise, the only general solution is $\tilde{h}_{2,4} = 0$ *unless* the system is degenerate, in which case there is a family of non-trivial solutions. This condition yields:

$$c^4 - c^2(c_1^2 + c_3^2) + c_1^2 c_3^2\left(1 - \frac{\rho_3}{\rho_1}\right) = 0,$$

with $c_{1,3}^2 = gH_{r1,3}$, are the gravity wave velocities associetd with the lower and upper layers. giving (first order to $1 - \frac{\rho_3}{\rho_1}$):

$$c_+^2 = c_1^2 + c_3^2, \quad c_-^2 \approx \left(1 - \frac{\rho_3}{\rho_1}\right)\frac{c_1^2 c_3^2}{c_1^2 + c_3^2}.$$

The $+$ mode is barotropic (behaves as one shallow layer), and the $-$ is baroclinic (both layers in antiphase) and *slow*. At the limit $H_{1r} \gg H_{3r}$ (thermocline on deep ocean), the baroclinic velocity approximates to

$$c_-^2 \approx c_3^2\left(1 - \frac{\rho_3}{\rho_1}\right) \stackrel{\text{def}}{=} g_r H_{r3},$$

where we have defined g_r the reduced gravity.

3.2.7 Gravity waves in a closed channel

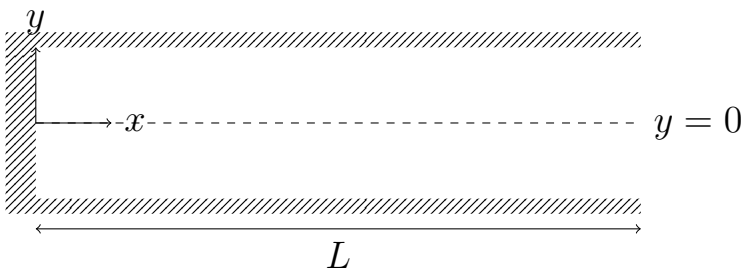

Consider shallow-water (Section 3.2.1) longitudinal gravity waves (along the x-axis) of the form

$$h(x,y,t) = \hat{h}^+ e^{i(kx+ct)} + \hat{h}^- e^{i(kx-ct)}$$
$$u(x,y,t) = \hat{u}^+ e^{i(kx+ct)} + \hat{u}^- e^{i(kx-ct)}$$

We consider, for simplicity, a solution $v = 0$ (l-wavenumber$= 0$). wavenumber Using the momentum conservation $\frac{\partial u}{\partial t} = -g\frac{\partial h}{\partial x}$, we have that $\hat{u}^\pm = \pm\frac{c}{H}\hat{h}^\pm$. Now, we consider that what we observe is the real part. Given that, say, $\hat{h}^+$ is a complex number, we write:

$$\text{Re}[\hat{h}^+ e^{i(kx+ct)}] = \hat{h}_c^+ \cos(kx+ct) - \hat{h}_s^+ \sin(kx+ct),$$

and likewise for the other terms. So, in this example, $h_c^+ = \text{Re}(\hat{h}^+)$ and $h_s^+ = -\text{Im}(\hat{h}^+)$. (Re and Im are the real-part and imaginary-part extractors, respectively.) Hence, the gravity wave solution is, for any k, fully defined by $\hat{h}_c^+$, $\hat{h}_s^+$, $\hat{h}_c^-$ and $\hat{h}_s^-$. These coefficients define the phases and amplitudes of the leftward and rightward components. However, using trigonometric identities (next page), it is possible to reparameterize this solution. It is possible to define components $h_{c,s}$ and phases $\phi_{1,2}$ such that (dropping the Real part operator):

$$h(x,y,t) = \hat{h}_c\left(\cos(kx)\cos(\omega t - \phi_1)\right) + \hat{h}_s\left(\sin(kx)\cos(\omega t - \phi_2)\right)$$

Using, again, the momentum conservation equation, we find, with this reparameterization:

$$u(x,y,t) = \frac{c}{H}\left[\hat{h}_c\left(\sin(kx)\sin(\omega t - \phi_1)\right) + \hat{h}_s\left(\cos(kx)\sin(\omega t - \phi_2)\right)\right]$$

With this reparameterization, we have exchanged our view of the solution as the combination of two progressive waves, with the view of the solution as a superposition of different stationary waves. These two views are

completely equivalent. This reparameterization is handy to account for the boundary conditions set by a closed channel, as shown in the figure. On the left-hand side, we impose a zero horizontal velocity, thus setting $\hat{h}_s = 0$. On the right-hand side (open sea), we impose a zero height, setting $\cos(kL) = 0$, that is $kL = \frac{\pi}{2} + m\pi$. Using the relationship $\omega = kc$ we find resonance frequencies in the channel ($\omega = 2\pi\nu$):

$$\nu = \frac{c}{2L}\left(m + \frac{1}{2}\right).$$

These eigenfrequencies are called "seiches". The problem of finding seiches in a lake can be solved analogously, imposing $u = 0$ on both ends.

(recall): Trigonometric identities

$$\cos u + \cos v = 2\cos\left(\frac{u+v}{2}\right)\cos\left(\frac{u-v}{2}\right)$$
$$\sin u + \sin v = 2\sin\left(\frac{u+v}{2}\right)\cos\left(\frac{u-v}{2}\right)$$
$$\sin u - \sin v = 2\cos\left(\frac{u+v}{2}\right)\sin\left(\frac{u-v}{2}\right)$$
$$\cos u - \cos v = -2\sin\left(\frac{u+v}{2}\right)\sin\left(\frac{u-v}{2}\right)$$

3.3 Quasi-hydrostatic waves in the f-plane

3.3.1 Vorticity equation in shallow water

The shallow-water version of the Euler equation is given in (SV-Hydro.2).
As velocities are horizontal, the vorticiy, $\zeta \overset{\text{def}}{=} \boldsymbol{\nabla} \times \boldsymbol{u}_h$, is a vertical vector.
We note $\boldsymbol{\zeta} = \zeta \boldsymbol{e}_z$.
The divergence of the horizontal component of velocity satisfies $\boldsymbol{\nabla} \cdot \boldsymbol{u}_h = -\frac{\mathrm{D}H}{\mathrm{D}t}$.
Furthermore, as vorticity and velocity are by design orthogonal to each other, $\boldsymbol{\zeta} \cdot \boldsymbol{\nabla} \boldsymbol{u}_h = 0$.
Doing similar operations as in subsection 3.1.3.3, but with $\boldsymbol{u}_h$, we find:

$$\begin{aligned} \boldsymbol{\nabla} \times \frac{\mathrm{D}\boldsymbol{u}_h}{\mathrm{D}t} &= \frac{\partial \boldsymbol{\zeta}}{\partial t} + \boldsymbol{u}_h \cdot \boldsymbol{\nabla} \zeta + \boldsymbol{\zeta} \boldsymbol{\nabla} \cdot \boldsymbol{u}_h \\ \boldsymbol{\nabla} \times (f \boldsymbol{e}_z \times \boldsymbol{u}_h) &= \boldsymbol{u}_h \cdot \boldsymbol{\nabla} f \boldsymbol{e}_z + f \boldsymbol{e}_z \boldsymbol{\nabla} \cdot \boldsymbol{u}_h \end{aligned}$$

Summing both identities, and identifying $\zeta_p \overset{\text{def}}{=} f$ and using $\boldsymbol{\nabla} \times \boldsymbol{\nabla} h = 0$:

$$\frac{\mathrm{D}\zeta_a}{\mathrm{D}t} + \zeta_a \boldsymbol{\nabla} \cdot \boldsymbol{u}_h = 0 \quad \Rightarrow \quad H \frac{\mathrm{D}\zeta_a}{\mathrm{D}t} - \zeta_a \frac{\mathrm{D}H}{\mathrm{D}t} = 0 \quad \Rightarrow$$

$$\frac{\mathrm{D}}{\mathrm{D}t} \left(\frac{\zeta_a}{H} \right) = 0. \tag{PVortCons}$$

The last equation expresses the conservation of potential vorticity.
A few elementary consequences:

- Lee depression after air stream passing over a hill
- Barotropic oscillations when contending a montain range (barotropic Rossby waves)

The unit of potential vorticity is $\mathrm{s}^{-1}\mathrm{m}^{-1}$.

3.3.2 Geostrophic velocity

3.3.3 Poincaré Waves (f-plane)

Take first, the shallow-water vorticity equation, in the $f-$plane (f constant), linearised (we drop tildes for ease of notation):

$$\frac{\partial}{\partial t}\left(\zeta - \frac{f}{H_r}h\right) = 0.$$

This is the linear version of potential vorticity conservation, in the $f-$plane. As we consider only fluctations, this constant anomalous potential vorticity (associated with fluctuations) must be zero, thus $\zeta = \frac{f}{H_r}h$.

As we have seen above, the *rotational* of the velocity equation gives (linearised):

$$\frac{\partial \zeta}{\partial t} = -f\delta, \quad \text{with } \delta \stackrel{\text{def}}{=} \boldsymbol{\nabla} \cdot \boldsymbol{u}_h. \tag{3.4}$$

Now, if we take the *divergence* of the velocity equation, we obtain (in the linear form):

$$\frac{\partial \delta}{\partial t} = f\zeta - g\nabla^2 h = f\zeta - \frac{c^2}{f}\nabla^2\zeta, \text{with } c_g^2 = gH_r.$$

This is the linear version of the vorticity equation. The symbol c_g stands for the velocity of gravity waves.

Combining both, we get one second-order differential equation for ζ:

$$\frac{\partial^2 \zeta}{\partial t^2} = -f^2\zeta + c_g^2\nabla^2\zeta.$$

Assuming a progressive wave form, we get the dispersion relation

$$\omega^2 = c_g^2 k^2 + f^2.$$

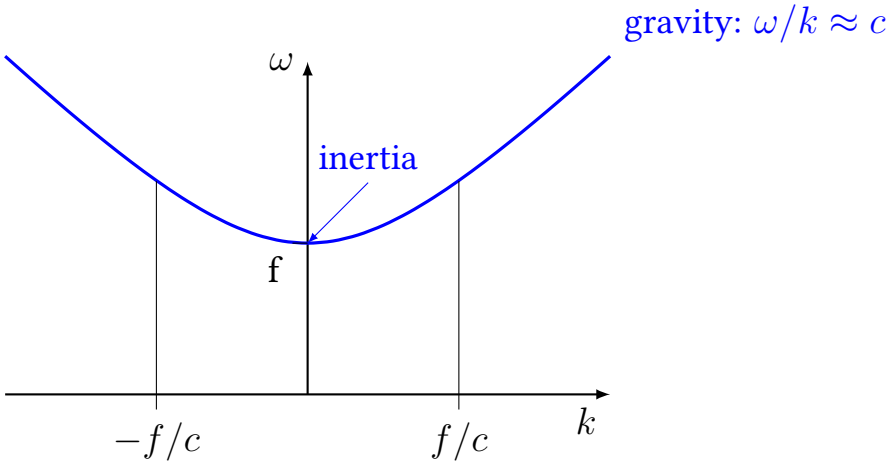

The transition between inertia regime and gravity occurs for $1/k = L_r$, where $L_r \overset{\text{def}}{=} c_g/f$.

3.3.4 Kelvin waves

The Kelvin waves are obtained from the quasi-hydrostatic Saint-Venant model. Impose $v = 0$ in the movement equations. We have (linearised)

$$\begin{aligned} \frac{\partial u}{\partial t} &= -g\frac{\partial h}{\partial x} \\ \frac{1}{H}\frac{\partial u}{\partial x} &= -\frac{\partial h}{\partial t} \end{aligned}$$

Thus, in the x-direction, we have exactly the same conditions as obtained for a gravity wave, with two solutions travelling a priori either eastwards or westwards. If we use the usual plane-wave solution, we are looking for solutions of the form: $h(x,y,t) = \hat{h}^+(y)e^{ik(x+ct)} + \hat{h}^-(y)e^{ik(x-ct)}$, and similar for u. Plugging this solution in the equation one of the two equations, we get:

$$\begin{aligned} \hat{u}^+(y) &= c/Hh^+(y) \\ \hat{u}^-(y) &= -c/Hh^+(y) \end{aligned}$$

The y-dependence is imposed by the diagnostic force balance in the y-direction $fu = -g\frac{\partial h}{\partial y}$. We find:

$$\frac{\mathrm{d}h^+}{\mathrm{d}y} = \frac{1}{L_r}h^+, \quad \frac{\mathrm{d}h^-}{\mathrm{d}y} = -\frac{1}{L_r}h^-.$$

giving

$$h = \hat{\hat{h}}^+ e^{y/L_R} e^{ik(x+ct)} + \hat{\hat{h}}^- e^{-y/L_R} e^{ik(x+ct)}.$$

In a channel, both components can propagate. If we have only one wall, e.g., at $x = 0$, then only the h^--wave can propagate, leaving the wall on its right-hand-side (in the northern hemisphere). As this is valid for all k, this is generalisable to a wave packet (sum of k-components).

3.4 Quasi-geostrophic barotropic waves in the β-plane

3.4.1 Geostrophic wind in the f-plane

The geostrophic wind or velocity is a diagnostic quantity, defined such as to satisfy the geostrophic balance which, in the shallow-water model, is $f\boldsymbol{e}_z \times \boldsymbol{u}_{gh} = -g\boldsymbol{\nabla} h$. We therefore have:

$$\boldsymbol{u}_{gh} \stackrel{\text{def}}{=} \frac{g}{f}\boldsymbol{e}_z \times \boldsymbol{\nabla} h.$$

If f is constant (f-plane approximation), we can rewrite $\boldsymbol{u}_{gh} = \boldsymbol{e}_z \times \frac{g}{f}\boldsymbol{\nabla} h$ which basically states that $\psi \stackrel{\text{def}}{=} \frac{g}{f}h$ acts as a vector potential ($\boldsymbol{e}_z \times \boldsymbol{\nabla}\psi = -\boldsymbol{\nabla} \times \psi\boldsymbol{e}_z$).
One of the consequences is that $\boldsymbol{u}_{gh}$ is non divergent, and that $\boldsymbol{\nabla} \times \boldsymbol{u}_{gh} = \nabla^2\psi$. There is thus an immediate connection between the pressure field and geostrophic vorticity: a high pressure (local maximum) corresponds to a negative vorticity (anti-cyclonic).

3.4.2 Geostrophic reference in the mid-latitude β-plane

The β-plane approximation is a first-order approximation around a standard $f = f_0$: $f = f_0 + \beta y$ where $\beta = \frac{\mathrm{d}f}{\mathrm{d}y}$.
We then define the β-plane geostrophic reference as:

$$\boldsymbol{u}_{gh} \stackrel{\text{def}}{=} \frac{g}{f_0}\boldsymbol{e}_z \times \boldsymbol{\nabla} h.$$

This is not quite the same as the actual geostrophic wind (it does not balance the pressure gradient, except for $f = f_0$), but it retains the nice properties of non-divergence and still derives from a potential vector.
Hence, we define the β-plane ageostrophic wind as

$$\boldsymbol{u}_a = \boldsymbol{u}_h - \boldsymbol{u}_{gh},$$

3.4.3 Quasi-geostrophic flow in shallow-water

The quasi-geostrophic approximation of the shallow-water equations are:

$$H\boldsymbol{\nabla}\cdot\boldsymbol{u}_h = -\left.\frac{\mathrm{D}H}{\mathrm{D}t}\right|_g$$

$$\left.\frac{\mathrm{D}\boldsymbol{u}_g}{\mathrm{D}t}\right|_g + f_0\boldsymbol{e}_z\times\boldsymbol{u}_h + \beta y\boldsymbol{e}_z\times\boldsymbol{u}_g = -g\boldsymbol{\nabla}h$$

where we have defined the quasi-geostrophic material derivative as $\left.\frac{\mathrm{D}a}{\mathrm{D}t}\right|_g = \frac{\partial a}{\partial t} + \boldsymbol{u}_g\cdot\boldsymbol{\nabla}a$ (we neglect the advection by the ageostrophic component of the wind).
The quasi-geostrophic approximation neglects :

- the β effect associated with the ageostrophic component,
- the time (material) derivative of the ageostrophic component.
- advection by the ageostrophic component

Given the definition of the geostrophic wind in the β-plane, and remembering that the geostrophic component of the wind is non-divergent, the equations reduce to (neglecting $(H-H_r)(\boldsymbol{\nabla}\cdot\boldsymbol{u}_a)$):

$$H_r\boldsymbol{\nabla}\cdot\boldsymbol{u}_a = -\left.\frac{\mathrm{D}H}{\mathrm{D}t}\right|_g \tag{SW.QG.1}$$

$$\left.\frac{\mathrm{D}}{\mathrm{D}t}\right|_g \boldsymbol{u}_g + f_0\boldsymbol{e}_z\times\boldsymbol{u}_a + \beta y\boldsymbol{e}_z\times\boldsymbol{u}_g = 0. \tag{SW.QG.2}$$

If we further take the curl of (SW.QG.2) and project on the vertical axis, we obtain an equation for the quasi-geostrophic vorticity $\zeta_g \overset{\text{def}}{=} (\boldsymbol{\nabla}\times\boldsymbol{u}_g)\cdot\boldsymbol{e}_z$:

$$\left.\frac{\mathrm{D}}{\mathrm{D}t}\right|_g (f_0+\beta y+\zeta_g) + f_0\boldsymbol{\nabla}\cdot\boldsymbol{u}_a = 0.$$

Using the definition $\psi = gh/f$ and $H = h - b$ (b, the layer bottom), and using (SW.QG.1) to eliminate the velocity divergence:

$$\left.\frac{\mathrm{D}}{\mathrm{D}t}\right|_g \left(\nabla^2\psi + (f_0+\beta y) - \frac{f_0^2}{gH_r}\psi + \frac{f_0}{H_r}b\right) = 0 \tag{SW.QGPV}$$

This expresses the conservation of quasi-geostrophic, potential vorticity, in the shallow-water realm.
The factor $\sqrt{\frac{gH_r}{f_0}^2}$ has units of meters: it expresses the typical curls of ψ which, in the stationary case, achives the quasi-geostrophic balance expressed by (SW.QGPV). This is the *external* Rossby deformation radius.

$$R_d = \sqrt{\frac{gH_r}{f_0}^2}. \tag{3.5}$$

Key Outcome: Kleinschmidt invertibility principle

(SW.QG.1) and (SW.QG.2) tell us that the field of ψ, the potential vorticity encapsulates both the movement and the thickness. Both conservation of movement and mass involve the same quantity and no other variable. This has two consequences

- They provide the basis to understand the intertwined roles of mass advection and vorticity conservation in the development of waves and instabilities;
- The whole dynamics are described by the partial differential equation involving a single scalar field: ψ.

The latter is called the Kleinschmidt invertibility principle (based on a 1957 book chapter by E. Kleinschmidt).

3.4.4 Quasi-geostrophic flow in pressure coordinates

Most of the development of subsection 3.4.3 is valid outside the specific realm of the shallow-water approximation. The geostrophic flow may either be expressed on a horizontal (constant geopotential Φ), or on a isobar (constant pressure p).
In the atmosphere, it is common to work in isobar coordinates. The vertical coordinate is pressure, and the equivalent of vertical velocity is the material derivative of pressure

$$\frac{\mathrm{D}p}{\mathrm{D}t} \overset{\text{def}}{=} \omega \tag{omega}$$

The continuity equation becomes

$$\boldsymbol{\nabla} \cdot \boldsymbol{u}_a = \frac{\partial \omega}{\partial p} \qquad \text{(Cont.pr)}$$

The quasi-geostrophic potential vorticity, which is conserved is:

$$q_p \overset{\text{def}}{=} \left(\frac{1}{f_0} \nabla^2 \Phi + f + f_0 \frac{\partial \omega}{\partial p} \right). \qquad (3.6)$$

The quasi-geostrophic flow theory goes a little bit further, by considering conservation of heat (J is the diabatic heating, c_p the heat capacity at constant pressure, θ the potential temperature)). The heat conservation accounts for the adiabatic expansion associated with the vertical movement. The parameter S_p is the static stability.

$$\frac{\mathrm{D}T}{\mathrm{D}t} = \frac{J}{c_p} - S_p \omega, , \quad \text{with } S_p \overset{\text{def}}{=} -T \frac{\partial \ln \theta}{\partial p}$$

In the quasi-geostrophic approximation we consider only the advection by the geostrophic wind:

$$\left. \frac{\mathrm{D}T}{\mathrm{D}t} \right|_g - S_p \omega = \frac{J}{c_p}$$

The temperature term is converted into density using the perfect gaz assumption, and density is then eliminated using the hydrostatic assumption, that is:

$$\frac{R_a T}{p} = \frac{1}{\rho} = -\frac{\partial \Phi}{\partial p}$$

We further define a reference static stability term corresponding to the basic state of the atmosphere

$$\sigma \overset{\text{def}}{=} -\frac{R T_0}{p} \frac{\mathrm{d} \ln \theta_0}{\mathrm{d}p}.$$

These different assumptions and definitions allow to re-express the dynamics of the quasi-geostrophic flow as a single equation involving solely the geopotential. Indeed, we isolate ω in the heat conservation equation, plug it in the potential vorticity to obtain

$$\left.\frac{\mathrm{D}q}{\mathrm{D}t}\right|_g = -\frac{R_a f_0}{p\sigma c_p}\frac{\partial J}{\partial p}, \quad \text{with } q = \left(\frac{1}{f_0}\nabla^2\Phi + f + \frac{\partial}{\partial p}\left(\frac{f_0}{\sigma}\frac{\partial \Phi}{\partial p}\right)\right), \tag{QGflow}$$

and $\boldsymbol{u}_g = \frac{1}{f_0}\boldsymbol{e}_z \times \nabla\Phi$.
todo: re-express things as a function of the Brunt-Vaisaala frequency

3.4.5 TODO : Quasi-geostrophic flow in horizontal coordinates

A FAIRE, POUR ENSUITE REMPLACER LA SECTION 3.7.1 OU DU MOINS LA RENDRE PLUS SUCCINCTE VEILLER AUSSI A LA COHERENCE DES NOTATIONS

3.4.6 Shallow-water rossby waves in the extratropical β-plane

We come back to the shallow-water geostrophic flow of subsection 3.4.3. Using again $f = f_0 + \beta y$, $u = u_g + u_a$, $v = v_g + v_a$, the shallow-water equations linearised around a rest ($\boldsymbol{u}_h = 0$) state are:

$$\begin{aligned}
&\frac{\partial u_g}{\partial t} - f_0 v_a - \beta y v_g = 0,\\
&\frac{\partial v_g}{\partial t} + f_0 u_a + \beta y u_g = 0,\\
&\frac{\partial h}{\partial t} = H_0\left(\frac{\partial u}{\partial x} + \frac{\partial v}{\partial y}\right).
\end{aligned}$$

Combine the first two equations to express the curl of $\boldsymbol{u}_g$, and use the third equation to replace the ageostrophic wind divergence which will appear (and remember that the geostrophic wind is non-divergent). Assume also a flat bottom:

$$\frac{\partial \zeta_g}{\partial t} + \beta v_g = \frac{f_0}{H_0}\frac{\partial h}{\partial t}$$

At this point, express everything as a function of h (this is the typical quasi-geostrophic strategy):

$$\frac{g}{f_0}\frac{\partial \nabla^2 h}{\partial t} + \beta \frac{g}{f_0}\frac{\partial h}{\partial x} = \frac{f_0}{H_0}\frac{\partial h}{\partial t}.$$

Multiply by f_0 and use $c^2 = gH_0$ to obtain:

$$\frac{\partial \nabla^2 h}{\partial t} + \beta \frac{\partial h}{\partial x} = \frac{f_0^2}{c^2}\frac{\partial h}{\partial t}.$$

Plug the plane-wave solution $h = \hat{h}e^{i(kx+ly-\omega t)}$ to obtain the dispersion relation:

$$\omega = -\frac{\beta k}{k^2 + l^2 + f_0^2/c^2}$$

thus, the phase velocity is

$$c_p = -\frac{\beta}{k^2 + l^2 + f_0^2/c^2}$$

If we now assume that these waves are superimposed on a mean flow (which we can assume with the linear approximation), drifting with an eastward velocity U, the phase velocity with respect to the ground is:

$$c_p = U - \frac{\beta}{k^2 + l^2 + f_0^2/c^2}$$

there exists thus a wavelength corresponding to the stationary wave ($c_p = 0$):

$$k_h^2 = \frac{\beta}{U} - f_0^2/c^2$$

exercise: compute the typical wavelength corresponding to stationary waves at mid-latitudes.

The dispersion relationship can be rewritten as follows:

$$(k + \beta/2\omega)^2 + l^2 = \left(\frac{\beta}{2\omega}\right)^2 - \left(\frac{f_0}{c}\right)^2.$$

in other words, lines of equal ω are circles in the (k, l) plane, centred on $(-\frac{\beta}{2\omega}, 0)$ and of radius $\sqrt{\left(\frac{\beta}{2\omega}\right)^2 - \left(\frac{f_0}{c}\right)^2}$.
As group-velocity is the gradient of ω in the (k, l) plane, group-velocity vectors are directed towards the center of the circles.
The line deviding eastward-propagating from westward-propagating waves (in the group-velocity sense) is the hyperbola defined by

$$k^2 = l^2 + \left(\frac{f_0}{c}\right)^2$$

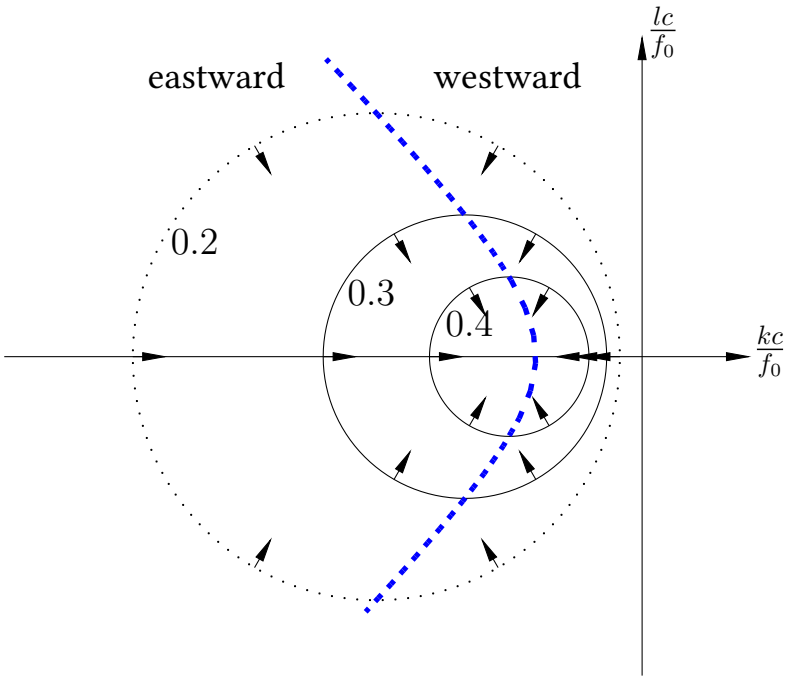

3.5 Quasi-hydrostatic waves in the equatorial β-plane

3.5.1 Shallow-water equations in the equatorial β-plane

The equator effectively acts as a waveguide due to the Coriolis factor changing sign at the equator. This forms the basis for explaining important phenomena such as El Niño and the Madden-Julian oscillation. The β-plane approximation around the equator reads:

$$f = 2\Omega \sin\phi \approx 2\Omega\phi = \beta y; \quad \beta \overset{\text{def}}{=} 2\Omega/R, \tag{3.7}$$

with R, the Earth's radius.

Baroclinic Instability in the β-Plane

Develop the quasi-hydrostatic shallow-water equations in the β-plane approximation

The quasi-hydrostatic shallow-water equations in the β-plane approximation are linearized around the still equilibrium:

$$H_0\left(\frac{\partial u}{\partial x} + \frac{\partial v}{\partial y}\right) + \frac{\partial h}{\partial t} = 0 \tag{3.8a}$$

$$\frac{\partial u}{\partial t} - \beta y v + g\frac{\partial h}{\partial x} = 0 \tag{3.8b}$$

$$\frac{\partial v}{\partial t} + \beta y u + g\frac{\partial h}{\partial y} = 0. \tag{3.8c}$$

(We omitted the tildes for simplicity.) We also use the potential vorticity conservation: (PVortCons), again linearized in the β plane:

$$\frac{\partial}{\partial t}\left(\zeta - \frac{\beta y}{H_0}h\right) = 0. \tag{3.9}$$

It is possible, based on the above, to eliminate all terms in u and h by performing the following:

$$\begin{aligned} &-\frac{\beta y}{c_g^2}\frac{\partial}{\partial t}(3.8b) + \frac{1}{c_g^2}\frac{\partial^2}{\partial t^2}(3.8c) - \frac{1}{H_0}\frac{\partial^2}{\partial y \partial t}(3.8a) - \frac{\partial}{\partial x}(3.9) \Rightarrow \\ &\frac{\partial}{\partial t}\left\{\frac{1}{c_g^2}\left(\frac{\partial^2 v}{\partial t^2} + f^2 v\right) - \left(\frac{\partial^2 v}{\partial x^2} + \frac{\partial^2 v}{\partial y^2}\right)\right\} - \beta\frac{\partial v}{\partial x} = 0. \end{aligned} \tag{3.10}$$

where $c_g^2 \overset{\text{def}}{=} gH_0$ is the gravity-wave velocity. This will be our fundamental equation.

3.5.2 Equatorial Kelvin waves

Equatorial Kelvin waves are the simplest to obtain: they are the trivial solution of (3.10) with $v = 0$. Imposing this solution in (3.8) leaves:

$$H_0 \frac{\partial u}{\partial x} + \frac{\partial h}{\partial t} = 0, \quad \frac{\partial u}{\partial t} + g\frac{\partial h}{\partial x} = 0 \tag{3.11}$$

$$\beta y u + g\frac{\partial h}{\partial y} = 0. \tag{3.12}$$

These equations have the advantage of being well "separated" in x and y. The first two equations (3.11) suggest plane wave propagation in the $\boldsymbol{e}_x$ direction:

$$\begin{aligned} u &= \hat{u}(y)\exp[i(kx - \omega t)] \\ h &= \hat{h}(y)\exp[i(kx - \omega t)] \end{aligned} \tag{3.13}$$

Combining (3.13) and (3.11) yields:

$$u = \frac{g}{c}h; \quad \omega = kc. \tag{3.14}$$

These waves are therefore non-dispersive ($c_p = c_{\text{group}} = c$). Solving the differential equation in y (3.12) gives:

$$\hat{h}(y) = \exp\left(-\frac{\beta y^2}{2c}\right). \tag{3.15}$$

The profile of the Kelvin wave in the meridional axis is thus a Gaussian centered at the equator. Its characteristic width is:

$$\sqrt{2}L_e; \quad L_e \overset{\text{def}}{=} \sqrt{c/2\beta} \tag{3.16}$$

The quantity L_e is called the equatorial Rossby deformation radius. For barotropic ocean waves, its value is on the order of 2000 km, which is somewhat large for the β-plane hypothesis. However, for baroclinic waves ($c \approx 0.5 - 3\ \mathrm{m\,s^{-1}}$), the radius ranges from 650 to 1300 km, which is perfectly acceptable. Under these conditions, a baroclinic Kelvin wave can cross the Pacific in about 2 months.

3.5.3 Equatorial Rossby waves and other solutions

The differential equation (3.10) admits other solutions. Again, we seek progressive waves, so we can try the following form:

$$v = \hat{v}(y)\exp[i(kx - \omega t)] \tag{3.17}$$

This form does not allow us to find all solutions, but we will find the most relevant ones. Equation (3.10) reduces in this case to an ordinary differential equation:

$$\frac{\partial^2 \hat{v}}{\partial y^2} + \left(\frac{\omega^2}{c^2} - k^2 - \frac{\beta k}{\omega} - \frac{\beta^2 y^2}{c^2}\right)\hat{v} = 0 \tag{3.18}$$

This equation is nonlinear and quite difficult. It is a Weber differential equation. Fortunately, it has been studied long before us. We seek solutions that vanish far from the equator, i.e., $\lim_{y\to\pm\infty}\hat{v} = 0$. If we define n and z by the following relations:

$$\frac{2\beta}{c}\left(n + \frac{1}{2}\right) \equiv \left(\frac{\omega}{c}\right)^2 - k^2 - \frac{\beta k}{\omega} \tag{3.19}$$

$$z := \sqrt{\frac{2\beta}{c}}y \tag{3.20}$$

then the solution is known as the parabolic cylinder function:

$$\hat{v} = D_n(z) \tag{3.21}$$

This means there exists a solution to the differential equation for v for each value of n. Only solutions for $n \geq 0$ vanish as $z \to \pm\infty$ and are thus admissible. The relation (3.19) then plays the role of the dispersion relation. Moreover, a simple analytical form exists for waves such that n is a non-negative integer. It has been shown that in this case, the function D reduces to a form better known to physicists, involving the Hermite polynomial:

$$\hat{v} = 2^{-n/2}\exp(-z^2)H_n(z) \tag{3.22}$$

For reference, the Hermite polynomials are: $H_0(z) = 1$, $H_1(z) = z$, $H_2(z) = 4z^2 - 1$, $H_3(z) = z^3 - 3z$, etc. Thus, for $n = 0$, $\hat{v}$ takes the form of a Gaussian. This means the horizontal motion corresponds to a

back-and-forth motion across the equator. The wave obeys the dispersion relation:

$$\frac{\omega}{c} - k - \frac{\beta}{\omega} = 0 \Leftrightarrow k = \frac{\omega}{c} - \frac{\beta}{\omega} \tag{3.23}$$

We will return later to the properties of this wave, but note that there exists a critical frequency such that $\omega = \sqrt{\beta c}$, for which the wave is stationary and fully invariant in the $\boldsymbol{e}_x$ direction. The corresponding period is 9 days to 3 weeks in the ocean (depending on the depth of the layer considered for the baroclinic mode), and about 5 days for the atmosphere.

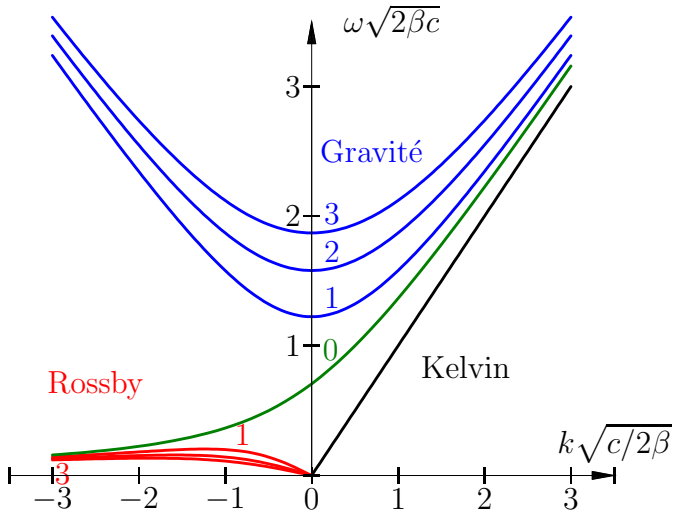

Figure 3.1: Dispersion relations of tropical waves

For $n \geq 1$, we see that the dispersion relation (3.19) can be satisfied for ω either large (the first term on the right dominates) or small (the third term dominates). In the first case, we approximately have:

$$\omega^2 \approx (2n+1)\beta c + k^2 c^2 \tag{3.24}$$

This form resembles Poincaré waves. This is why they are sometimes called equatorial Poincaré waves, or equatorial gravity waves. They appear for both positive and negative k and can thus propagate both eastward and westward.

In the second case, we have:

$$\omega \approx -\frac{\beta k}{k^2 + \frac{(2n+1)\beta}{c}}. \tag{3.25}$$

Here, k and ω have opposite signs. These are necessarily waves with a westward phase velocity. The group velocity is also westward but very weak. This means such a wave, if baroclinic, can take a year to cross the Pacific basin. These waves share the same characteristics as the Rossby waves found in 3.4, which is why they are called equatorial Rossby waves, or equatorial planetary waves.
Let us now return to the $n = 0$ wave: it behaves like a Poincaré wave for large positive k and like a planetary Rossby wave for negative k. It is therefore called a mixed planetary-gravity wave. The phase velocity can be eastward or westward, but the group velocity is always directed eastward.

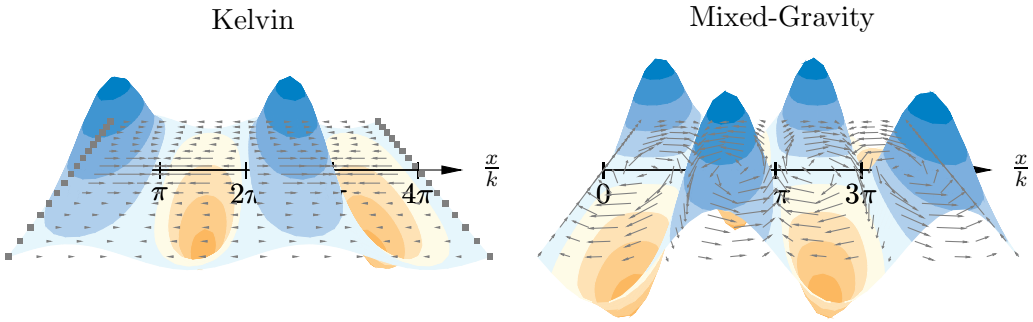

Figure 3.2: Height and velocity fields associated with Kelvin waves and tropical mixed gravity waves, assuming $k^2 = c/(2\beta)$.

3.6 Kelvin-Helmoltz instability

In the linear framework, wave instability is manifested by a imaginary part in the velocity c, as it generates a real exponential in $e^{ix(x-ct)}$. Instability must grow on a source of energy, which is generally supplied by a gradient of velocity or a gradient of potential energy.

The classical theory considers an interface between two layers, and the resolution of the solution produces a dispersion relationship.

We consider an interface between two deep layers (below and above the reference line $z = 0$, and both deep layers have horizontal velocities $\boldsymbol{U}_1$ and $\boldsymbol{U}_3$, only. We consider the problem in the $x - z$ plane only, so $\boldsymbol{U}_{1,3} = U_{1,3}\boldsymbol{e}_x$. Both layers extend infinitely to the top and bottom. The deviation at the interface with respect to the $z = 0$ line is η.

Compared to the formulation of section 3.2.6 we consider explicitly the transfer of momentum at the surface, and surface tension. One simple way to do this is to consider the (Bernoulli) equation at the interface, and consider the perturbation as non-rotational (because firt-order effects do not create vorticity), that is:

$$(u_1, w_1) = \boldsymbol{U}_1 + \boldsymbol{\nabla}\varphi_1$$
$$(u_3, w_3) = \boldsymbol{U}_3 + \boldsymbol{\nabla}\varphi_3$$

and

$$\boldsymbol{\nabla}\left(\rho_1\frac{\partial\varphi_1}{\partial t} + \left(\frac{\partial\varphi_1}{\partial x}\right)^2 + \left(\frac{\partial\varphi_1}{\partial z}\right)^2 + g\eta + p_1\right) = 0$$
$$\boldsymbol{\nabla}\left(\rho_3\frac{\partial\varphi_3}{\partial t} + \left(\frac{\partial\varphi_3}{\partial x}\right)^2 + \left(\frac{\partial\varphi_3}{\partial z}\right)^2 + g\eta + p_3\right) = 0$$

The difference between the two terms under the gradient operator is constant in space, and can be set to zero given the flexibility given by the choice of potential velocities.

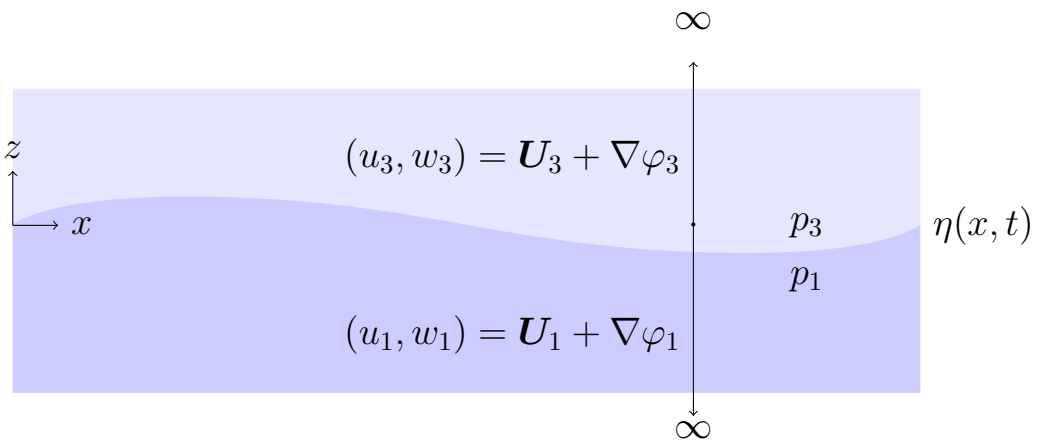

The pressure difference is set by the surface tension:

$$p_1 - p_3 = T\frac{\partial^2\eta}{\partial x^2}.$$

To close the system, we need, first, to express the link between vertical and horizontal velocities. This is the vertically-integrated continuity equation assuming a Boussinesq flow, keeping again first-order terms in the perturbation only:

$$\frac{\partial\eta}{\partial t} + U_1\frac{\partial\eta}{\partial x} = w_1 = \frac{\partial\varphi}{\partial y}_1$$
$$\frac{\partial\eta}{\partial t} + U_3\frac{\partial\eta}{\partial x} = w_3 = \frac{\partial\varphi}{\partial y}_3$$

Keeping, again, first order terms, we get the master equation

$$\rho_1\left(\frac{\partial\varphi}{\partial t} + U_1\frac{\partial\varphi}{\partial x}\right) + (\rho_1 - \rho_3)g\eta = \rho_2\left(\frac{\partial\varphi}{\partial t} + U_2\frac{\partial\varphi}{\partial x}\right) + T\frac{\partial^2\eta}{\partial x^2}.$$

We try a horizontal progressive wave solution, and the non-divergent flow imposes respecting the Laplace equation. Further imposing the disturbance to vanish at $z \pm \infty$ imposes the form:

$$\varphi_1(x,y) = \hat{\varphi}\exp(ik(x-ct))e^{y} \quad (y<0),$$
$$\varphi_3(x,y) = \hat{\varphi}\exp(ik(x-ct))e^{-y} \quad (y>0),$$

Plugging in the master equation generates the dispersion constrain:

$$\omega = \frac{\rho_1 U_1 + \rho_2 U_2}{\rho_1+\rho_2}k \pm \sqrt{\frac{-\rho_1\rho_3(U_1-U_3)^2}{(\rho_1+\rho_3)^2} + g(k)k^2}$$

with

$$g(k) = \frac{\rho_1-\rho_2}{\rho_1+\rho_2}\frac{g}{k} + \frac{T}{\rho_1+\rho_2}k$$

There is imaginary phase velocity, thus instability, when the term under the square root is negative. The first term is the horizontal shear. The second term balances the horizontal shear by vertical stability and surface tension.

There is always instability if $\rho_1 < \rho_3$, that is, the denser layer is on the top.

The linear theory does not tell us what happens when the instability develops. Its structure changes as non-linear terms kick-in, but we know that it takes the characteristic shape of large waves loved by surfers. It can also be rendered visible in clouds, as on this Wikicommon contribution oven Mount Duval, New South Wales

3.7 Baroclinic instability in the f-plane

3.7.1 Equations of a quasi-geostrophic perturbation with mean velocity shear

We consider the perturbation of a geostrophic flow with a reference velocity profile $\boldsymbol{U}(z)$. The perturbation has a geostrophic component $\boldsymbol{u}_g$ and an ageostrophic component $\boldsymbol{u}_a$, associated with vertical velocity w.
We adopt the streamfunction formalism for the geostrophic component of the perturbation $\boldsymbol{u}_g$, that is:

$$\boldsymbol{u}_g = \boldsymbol{e}_z \times \boldsymbol{\nabla}\psi$$

and the vorticity $\zeta = \nabla^2\psi$.
The vertical velocity is linked to the horizontal divergence by the continuity equation:

$$\frac{\partial w}{\partial z} = -\boldsymbol{\nabla}\cdot\boldsymbol{u}_a$$

This leads to the equation for the quasi-geostrophic vorticity balance in the f-plane (note: to be added in Sect. 4.2):

$$\left.\frac{\mathrm{D}}{\mathrm{D}t}\right|_g \nabla^2\psi = (\frac{\partial}{\partial t} + U(z)\frac{\partial}{\partial x})\nabla^2\psi = -f_0\frac{\partial w}{\partial z}. \tag{QG1}$$

We consider the equation for the conservation of heat, assuming no diabatic heating. That is, with entropy $s = \ln\theta$: $\frac{\mathrm{D}s}{\mathrm{D}t} = 0$, which, when expanded along the three dimensions, becomes:

$$\left.\frac{\mathrm{D}s}{\mathrm{D}t}\right|_g + w\frac{\partial s_r}{\partial z} = 0 \tag{HEAT}$$

We use the hydrostatic assumption and assume that the density is linked to the entropy s by a constant factor γ: $\partial p/\partial z = \rho_r\gamma(s - s_r)$, where ρ_r is the reference density. Furthermore, the geostrophic velocity is linked to the horizontal pressure gradient ($\boldsymbol{u}_g = \frac{1}{f_0}\boldsymbol{e}_z \times \nabla p/\rho_r$). It follows that:

$$\boldsymbol{\nabla}s = \frac{f_0}{\gamma}\boldsymbol{e}_z \times \frac{\partial \boldsymbol{u}_g}{\partial z} = \frac{f_0}{\gamma}\boldsymbol{e}_z \times (\boldsymbol{e}_z \times \boldsymbol{\nabla}\frac{\partial\psi}{\partial z}) = -\frac{f_0}{\gamma}\boldsymbol{\nabla}\frac{\partial\psi}{\partial z}. \tag{3.26}$$

The horizontal field of entropy s is thus linked to the vertical gradient of the streamfunction:

$$s = -\frac{f_0}{\gamma}\frac{\partial \psi}{\partial z} + C \tag{3.27}$$

such that (HEAT) becomes:

$$\left.\frac{\mathrm{D}}{\mathrm{D}t}\right|_g \frac{\partial \psi}{\partial z} = \frac{N^2}{f_0} w, \qquad N^2 \overset{\text{def}}{=} \gamma \frac{\partial s_r}{\partial z} \tag{QG2}$$

where the buoyancy frequency has already been defined on p. 38.
Equations (QG1) and (QG2) constitute the quasi-geostrophic perturbation with mean vertical velocity shear. The equations are given here in the f-plane for simplicity, and are developed in the β-plane in classical textbooks.

Key Outcome: Kleinschmidt invertibility revisited

Remember the Kleinschmidt invertibility principle seen in sect. 3.4.3, p. 49. It takes now a new dimension: potential vorticity encapsulates the movement and the *thermal structure*. Waves and instabilities emerge from the combined constraints of *heat* conservation and angular velocity conservation. This provides the basis to the particular structure of thermal and velocity fields in the mid-latitudes, as we show next.

3.7.2 Two-layer quasi-geostrophic model

[1] discretize the equations assuming a two-layer setup of height H_0 and density ρ, with reference velocities $\boldsymbol{U}_1$ (bottom) and $\boldsymbol{U}_3$ (top). The velocity shear is typically found at mid-latitudes as a consequence of the thermal wind relationship. A more refined model would consider a constant shear along the vertical, but we start with the two-layer formalism.

[1] The following development is based on N. Phillips' model Philips 1956 (cf. also Holton 2004, sect. 8.2, with one difference. Phillips' model is formulated in pressure coordinates, specifically adapted for the atmosphere. Thus, compared to what follows, the role of N^2 (Brunt–Väisälä frequency) is played by the static stability parameter $\sigma = N^2/(\rho_0 g)^2$, where ρ_0 is a reference density; the layer thickness is expressed as a pressure difference δp, and the factor λ, which is nothing other than the inverse of the Rossby deformation radius, is expressed as $f_0/(\sqrt{\sigma}\delta p)$. The vertical velocity is expressed using $\omega \overset{\text{def}}{=} \frac{\mathrm{D}p}{\mathrm{D}t}$, and finally, the entropy s is expressed directly as $C_p \ln \Theta$.

Let η be the vertical deviation at the interface, with $w_2 \overset{\text{def}}{=} \frac{\mathrm{D}\eta}{\mathrm{D}t}$. The top and bottom are fixed and flat, such that the quasi-geostrophic continuity equation reads:

$$\left.\frac{\mathrm{D}}{\mathrm{D}t}\right|_g (z_{\text{top}} - \eta) = \left.\frac{\mathrm{D}}{\mathrm{D}t}\right|_g (\eta - z_{\text{bottom}}) = -w_2.$$

For each layer, we use equation (QG1), approximating $\frac{\partial w}{\partial t}$ as $\mp w_2/H_0$:

$$\left(\frac{\partial}{\partial t} + \bar{U}_1 \frac{\partial}{\partial x}\right) \nabla^2 \psi_1 = -\frac{f_0}{H_0} w_2, \tag{3.28a}$$

$$\left(\frac{\partial}{\partial t} + \bar{U}_3 \frac{\partial}{\partial x}\right) \nabla^2 \psi_3 = +\frac{f_0}{H_0} w_2. \tag{3.28b}$$

We define mean and thermal quantities as follows:

$$\bar{U}_M = \frac{1}{2}(\bar{U}_1 + \bar{U}_3), \quad \bar{U}_T = \frac{1}{2}(\bar{U}_1 - \bar{U}_3). \tag{3.29}$$

We consider $\bar{U}_M$ as an approximation of the zonal velocity at the interface, $\bar{U}_2$, by interpolation, and $\bar{U}_T$ as an approximation of $H_0 \frac{\mathrm{d}\bar{U}}{\mathrm{d}z}$. The quantities ψ_M and ψ_T are defined analogously.
Using these relations, we can re-express ((3.28a) + (3.28b)) and ((3.28a) − (3.28b)) using (QG2). To avoid lengthy calculations, we now explicitly consider that the wave is zonal, so $\psi_y = 0$. This leaves:

$$\left(\frac{\partial}{\partial t} + \bar{U}_M \frac{\partial}{\partial x}\right) \frac{\partial^2 \psi_M}{\partial x^2} + \bar{U}_T \frac{\partial^2 \psi_T}{\partial x^2} = 0, \tag{3.30a}$$

$$\left(\frac{\partial}{\partial t} + \bar{U}_M \frac{\partial}{\partial x}\right) \left(\frac{\partial^2 \psi_T}{\partial x^2} - 2\lambda^2 \psi_T\right) + \bar{U}_T \left(\frac{\partial^2 \psi_M}{\partial x^2} + 2\lambda^2 \psi_M\right) = 0, \tag{3.30b}$$

where we set $\lambda \overset{\text{def}}{=} f_0/(NH_0)$.
We thus have a system of two partial differential equations. As usual, we "try" plane waves of the form $\psi = \hat{\psi} \exp(i(kx - \omega t))$. This yields a system of two coupled algebraic equations:

$$ik[(c_p - \bar{U}_M)k^2]\hat{\psi}_M - ik^3 \bar{U}_T \hat{\psi}_T = 0, \tag{3.31a}$$

$$ik[(c_p - \bar{U}_M)(k^2 + 2\lambda^2)]\hat{\psi}_T - ik\bar{U}_T(k^2 - 2\lambda^2)\hat{\psi}_M = 0, \tag{3.31b}$$

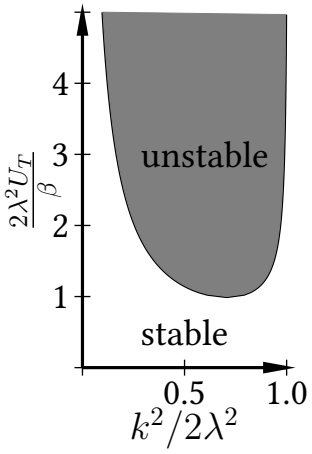

Figure 3.3: Instability condition in the Philips 1956 model

where, as a reminder, $c_p \overset{\text{def}}{=} \omega/k$. This homogeneous algebraic system admits non-trivial collinear solutions when the characteristic determinant vanishes, which, after calculation, leads to:

$$c_p = \bar{U}_M \pm \sqrt{\delta}, \quad \delta = -\bar{U}_T^2 \frac{2\lambda^2 - k^2}{k^2 + 2\lambda^2}. \tag{3.32}$$

We are faced with a very interesting situation. The velocity c_p has an imaginary solution as soon as $k^2 < 2\lambda^2$, since $\delta < 0$ in this case. This means that $\hat{\psi}$ will have at least one solution that grows exponentially. In other words, stratification stabilizes the shortest waves (since λ^2 is smaller as the fluid is more stratified), but all long waves are unstable.
We have thus proven that a flow with a horizontal gradient of mean temperature, satisfying the conditions of quasi-geostrophic flow, will almost always be unstable in the f-plane. In the β-plane, we would have obtained the following relation:

$$c_p = \bar{U}_M - \beta \frac{k^2 + \lambda^2}{k^2 + 2\lambda^2} \pm \sqrt{\delta}, \quad \delta = \frac{\beta \lambda^4}{k^2(k^2 + 2\lambda^2)} - \bar{U}_T^2 \frac{2\lambda^2 - k^2}{k^2 + 2\lambda^2}. \tag{3.33}$$

Here, we have a slightly different situation. The Earth's curvature has a stabilizing effect on planetary waves (small k). Only synoptic waves are unstable. They are indeed too small to benefit from the stabilizing effect of the Earth's curvature and too large to benefit from stratification.

In the special case $\beta = 0$, instability arises as soon as $2\lambda^2 - k^2 < 0$. Since $2\pi/k$ is the wavelength, the critical wavelength leading to instability is on the order of $\sqrt{2}\pi L_R$, where $L_R \overset{\text{def}}{=} 1/\lambda = NH_0/f_0$.
This is the *internal* Rossby deformation radius . Its expression differs from the definition (3.5), since role played by the factor $\sqrt{gH_0}$ is now played by NH_0. This is a fairly classic situation (see Holton, Sect. 8.2): the role played by $\sqrt{gH_0}$ (gravity wave speed) in a barotropic model is taken by NH_0 (characteristic speed associated with Brunt–Väisälä oscillations) in a model with vertical resolution (or $\sqrt{\sigma}\delta p$ if expressed in pressure coordinates.
Finally, note that if $\boldsymbol{U}_T = 0$, we recover the dispersion relation of Rossby waves. We then see that the phase velocity c_p admits two solutions:

$$c_1 = \bar{U}_M - \beta/k^2,$$
$$c_2 = \bar{U}_M - \beta/(k^2 + 2\lambda^2),$$

the first corresponding to the barotropic mode, the second to the baroclinic mode, where ψ_1 and ψ_3 are in antiphase.

3.7.3 Philip's theory in pressure coordinates

The original theory by Philips 1956 considered pressure layers in the atmosphere, typically two layers which are each 500 hPa, which avoids the uncomfortable assumption of a rigid top. All developments are the same : pressure plays the role of height and the horizontal gradient of pressure plays the role, in the equations, of the horizontal gradient of potential. This implies in particular that rather than considering vertical velocity w, we use the ω field, defined as the material derivative of pressure (downwelling parcels have positive ω).
Concretely, the important identities (3.32) are unchanged, but simply, the definition of λ is adapted to the pressure coordinates:

$$\lambda \overset{\text{def}}{=} \frac{f_0}{\sqrt{\sigma(\Delta p)^2}},$$

where σ is the static stability parameter in the isobaric framework $\sigma = -\frac{1}{\rho}\frac{\partial\theta}{\partial p}$, θ the potential temperature; and Δp the pressure difference between the two layers, 500 hPa.

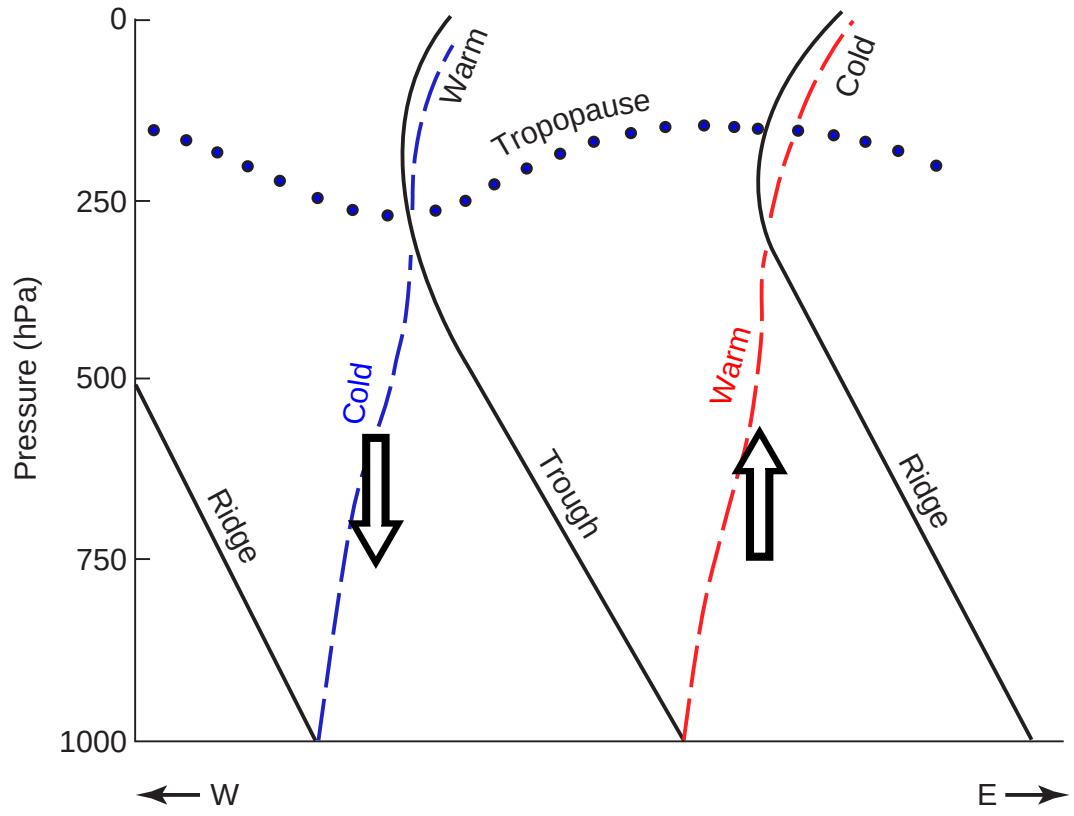

Figure 3.4: Redrawn for Fig. 6.6 in Holton p. 149

3.7.4 Interpretation of the baroclinic field

to do: based on Holton 2004, pp. 238 - 240

3.7.5 Eady problem

Still to do.

Chapter 4

Non-linear ocean-atmosphere phenomena

4.1 Beyond linearity with a modelling hierarchy

In the previous chapter we have relied an a well-established worflow to study waves and instabilities in the ocean or in the atmosphere: take equations of fluid motion adequate for the time-space context, linearise them, and study the dispersion relationship. In case of instability (imaginary part in the phase velocity), the linear model predicts exponential growth, which of course will only occur in the world until non-linear terms kick-in to potentially many outcomes: landing on another stable solution, oscillations, or chaos.

We are thus interested in understanding what happens beyond the instability. This is a difficult task. Of course, nonlinear partial differential equations can be solved numerically to observe the resulting dynamics. However, understanding — which we define here as the the ability to describe phenomena in terms of fundamental causes — is often achieved through the articulation of a hierarchy of models.

A landmark example is Saltzman's 1961 model Saltzman 1962, which transformed the convection problem into a system of ODEs by spectral truncation. This 12-ODE model was subsequently simplified by Lorenz and used in his celebrated publication Lorenz 1963, which demonstrated sensitive dependence on initial conditions. It has since become a textbook case, particularly because the model exhibits chaos when applied beyond its intended range of validity. Crucially for the general argument developed in this chapter, Lorenz showed that the chaotic behavior of his system mirrored the dynamics of the tent map, thereby moving through a nested modeling hierarchy: from PDEs to ODEs to deterministic iterations. While this hierarchical approach enhances understanding, it also introduces ambiguity, since different physical mechanisms may lead to mathematically similar equations.

The Saltzman model was designed to study atmospheric convection. Here, we focus on a phenomenon involving both the atmosphere and the ocean, beginning with an example in which the nonlinearity arises primarily from ocean dynamics: deep-decoupling oscillations. Although their phenomenology remains debated, they provide a valuable example of nonlinear behavior studied through a hierarchy of models, where simplified representations have played a central role in structuring scientific inquiry.

The history of deep-coupling oscillations is complex. Stommel, an oceanog-

rapher interested in global ocean circulation, proposed in 1961 a two-box model capturing essential processes driving the global ocean, particularly the Atlantic: the generation of buoyancy through exchanges of heat and freshwater with the atmosphere, and the advection of buoyancy by the large-scale circulation (Stommel 1961). By parameterizing advection as a function of the density difference between an equatorial and a polar box, he derived a system of two differential equations amenable to analysis using nonlinear dynamical methods, as discussed in LPHYS2264. The model exhibits saddle-node bifurcations, meaning that under certain conditions the system may reside either in an active (haline) circulation regime or in an inactive (thermal) one. This framework has strongly shaped our understanding of the potential risks associated with a future collapse of the thermohaline circulation.

In Stommel's model, the nonlinearity arises from the advective feedback loop: the advection of equatorial water enhances the density contrast that drives the circulation itself.

A further step was taken by Welander 1982, who also proposed a two-box model, this time arranged vertically. A similar configuration was previously examined in linear theory with stochastic forcing (REF), where the exchange coefficient between the upper and lower boxes was constant. In Welander's 1982 model, mass exchange becomes an on–off process conditioned on vertical instability: convection occurs when the density of the upper box exceeds that of the lower box. Within this framework, self-sustained oscillations can arise. Given the characteristic spatial scales involved, these oscillations typically have periods of a few years. Welander proposed them as a possible explanation for interannual to interdecadal variability in the North Atlantic. At that time, he had already published extensively on self-sustained oscillations in buoyancy-driven systems.

In a substantial book chapter, Welander 1986 later explored variations of the Stommel model and showed that some configurations generate oscillations. citewright91aa presented a two-dimensional (latitude–longitude, three-basin) quasi-geostrophic ocean model displaying at least transient regimes characterized by self-sustained oscillations with a typical duration of about 1000 years. Although the simulated dynamics lacked realism, they raised the possibility that convective adjustment and advective feedback could interact to generate oscillations. This point was particularly relevant at a time when Dansgaard–Oeschger oscillations were being

identified in paleoclimate records, and self-sustained oscillations appeared as a potential explanatory mechanism.
Winton and Sarachik developed a PDE-based model of the global ocean using a minimal friction-geostrophic framework to isolate the mechanisms underlying these oscillations (Winton and Sarachik 1993). In a book chapter published the same year, Winton 1993 interpreted these "deep-decoupling oscillations" using a three-box model that effectively combines Stommel's advective feedback with Welander's convective switching mechanism.

4.2 The Stommel two-box model

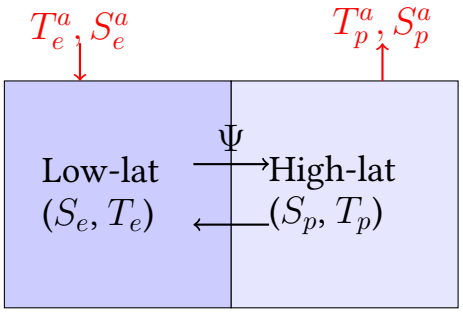

Based on Stommel 1961 we model the ocean as two well mixed boxes. The equatorial box has temperature and salinities (T_e and S_e), and the polar box (T_p and S_p). We consider restoring heat and freshwater fluxes conditions to reference temperature and salinities, as well has an advective flux that is determined by the density difference between the two boxes.
The original equation from Stommel 1961 consider the flux

$$\Psi = \gamma \frac{\rho_p - \rho_e}{\rho_0},$$

where ρ_0 is a reference density, and density anomalies are determined from the linear equation

$$\rho(T, S) = \rho_0(1 - \alpha_T(T - T_0) + \alpha_S(S - S_0))$$

The two-box design is specific and perhaps conteruintive in the sense that water is transferred from both boxes whether ψ is positive or negative. For example, the full equation for the polar box temperature is

$$V_p \frac{\mathrm{d}T_p}{\mathrm{d}t} = C_p^T (T_p^a - T_p) + |\Psi|(T_e - T_p),$$

where V_p is the box volume, C_p its specific heat, T_P^a is the reference air temperature for the computation of the net heat flux (first term); the second term is the advective flux.
Similarly, the polar salinity equation reads,

$$V_p \frac{\mathrm{d}S_p}{\mathrm{d}t} = C_p^S (S_p^a - S_p) + |\Psi|(S_e - S_p),$$

and so on for the equatorial box. After a-dimensionalisation and a first elimination of redundant equations the system reduces to two equations for the temperature and salinity differences between the two boxes:

$$\frac{\mathrm{d}T}{\mathrm{d}t} = \eta_1 - T(1 + |T - S|) \tag{4.1}$$

$$\frac{\mathrm{d}S}{\mathrm{d}t} = \eta_2 - S(\eta_3 + |T - S|) \tag{4.2}$$

Details and definitions are given in Dijkstra 2005, p. 66. Parameter η_1 is the intensity of the atmosphere thermal forcing, η_2, the salinity forcing (scaling with the difference $S_e - S_p$), and η_3 the ratio between the restoring time scales of temperature vs salinity (large η_s means quick salinity restoring).
A full analysis of equations (4.2) is given in Dijkstra 2005, sect. 3.1.2 and 3.1.3 and in Thual and Mcwilliams 1992. Crucial in this model is that it enacts a positive advective feedback: strong circulation produces strong buoyancy advection, which may enhance the density contrast and further strengthen the circulation. This generates the possibility of multiple states. We can see it in a few steps. Call $D = T - S$. The fixed points obey the relationships

$$T = \frac{\eta_1}{1 + |D|}, \quad S = \frac{\eta_2}{1 + |D|}, \quad D = T - S = \frac{\eta_1}{1 + |D|} - \frac{\eta_2}{\eta_3 + |D|},$$

The third equation is implicit. It may be rewritten as $F(D) = 0$ where

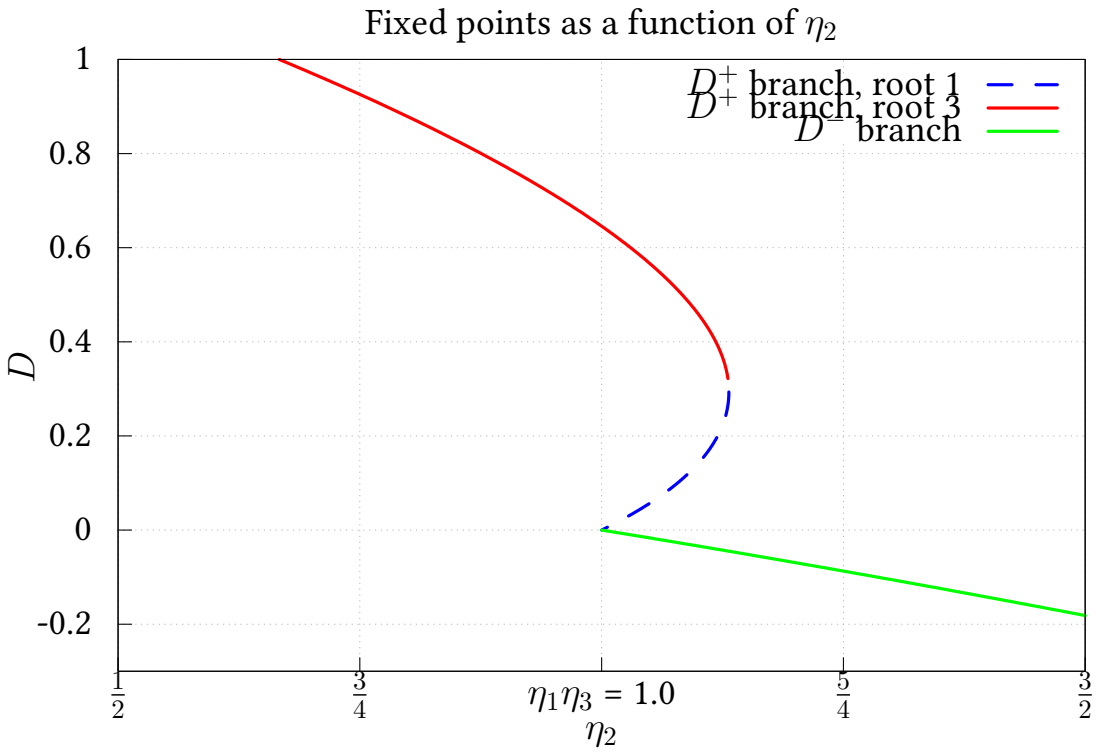

Figure 4.1: Bifurcation plot for $\eta_3 = 0.3$, $\eta_1 = 3.0$. The zero-crossing is at $\eta_2 = \eta_1\eta_3$. The right-hand-side bifurcation is available analytically; its form is quite complicated (cf. the `Stommel_maxima.ipynb` notebook).

$$F(D) = (1 + |D|)(1 + \eta_3|D|)D - \eta_1(\eta_3 + |D|) + \eta_2(1 + |D|)$$

There is a root (thus a solution) when $F(D) = 0$. There is a bifurcation when two roots merge in one, which also implies $F'(D) = 0$. The mathematical trick is to write both conditions $F(D) = 0$ and $F'(D) = 0$, and eliminate D, to obtain an equation for the parameters.

todo: discuss different regimes. ALso give the Rahmstorf (?) theory about the gyre vs deep ocean transport to determine whether we are in teh monostable or bistable regime.

4.3 The Winton Oscillator

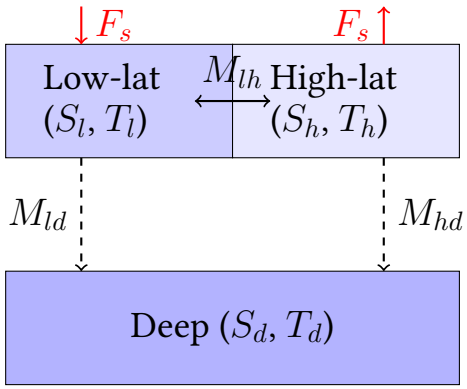

$$\frac{\mathrm{d}S_l}{\mathrm{d}t} = \frac{2M_{ld}}{hL}(S_d - S_l) + \frac{2M_{lh}}{hL}(S_h - S_l) + \frac{F_s}{h} \tag{4.3}$$

$$\frac{\mathrm{d}S_h}{\mathrm{d}t} = \frac{2M_{hd}}{hL}(S_d - S_h) + \frac{2M_{lh}}{hL}(S_l - S_h) - \frac{F_s}{h} \tag{4.4}$$

$$\frac{\mathrm{d}S_d}{\mathrm{d}t} = \frac{M_{ld}}{HL}(S_l - S_d) + M_{hd}HL(S_h - S_d) \tag{4.5}$$

$$\frac{\mathrm{d}T_d}{\mathrm{d}t} = \frac{M_{ld}}{HL}(T_l - T_d) + M_{hd}HL(T_h - T_d) \tag{4.6}$$

using $M_{\{l,h\}d} = C_{\{l,h\}}M_v$. $C_{\{l,h\}}$ are the convective parameters :

$$C_{\{l,h\}} = \begin{cases} 10 & \text{if } \rho(T_{\{l,h\}}, S_{\{l,h\}})\rho(T_d, S_d) \\ 1 & \text{else} \end{cases}$$

using the state function $\rho(T, S) = 0.79S - 0.0611T - 0.055T^2$. We take $h = 50\text{m}$, $H = 500\text{m}$, and the following mixing fluxes:

$$\frac{HL}{2M_v} = 200 \text{ years}, \qquad \frac{hL}{2M_{lh}} = 5 \text{ years}$$

T_l and T_h are fixed at 15°C and 0°C respectively.
todo: play with the jupyter notebook. What can of bifurcations acan we foreseen ?

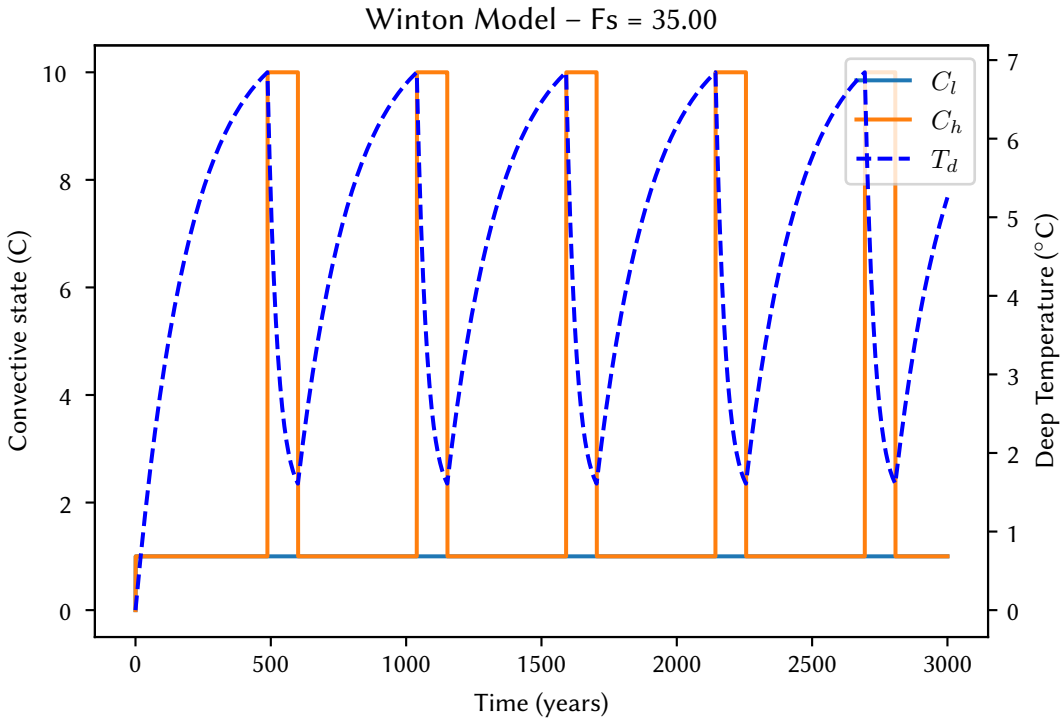

Figure 4.2: Oscillations in the Winton model

4.4 The El-Nino Southern Oscillation

The El-Nino Southern Oscillation is a pan-Pacific phenomenon characterised by a recurring positive and negative anomalies in the temperature of the Equatorial pacific. Warm anomalies — the El-Nino phase — are characterized by a decrease in downwelling and gloabl increase in the heat content in the mixed layer. This phase is most acute around the new year on the East coast of the Pacific. The opposite Nina phase is then characterised by increased upwelling and cold anomalies.
ENSO is a mode in the power spectrum density of Pacific Temperatures (e.g. Silva et al. 2020), with a typical recurring period of the order of 2 to 7 years. Each event is unique, but a robust distinction emerges between a "canonical" or "Central Pacific" El Nino and a "Modoki" El-Nino Takahashi et al. 2011.
An oscillation requires positive feedbacks. The Bjerkness feedback (named after Bjerknes 1969) connects a weakening of the trade winds in the Southern Hemisphere with a decresae in upwelling, thus a warm sea-surface temperature anomaly, which itself re-inforces the trade-wind anomaly. It is a key part of all theories. Delayed feedbacks occur consistently with the propagation of Kelvin and Rossby waves across the Pacific. Kelvin waves propogate Eastwards and cross the Pacific with a typical timescale of a month; the slower Rossby waves propagate Westwards, bounce back on the Western coasts and hits the West coast typically 6 months later. As we see here these dynamics are conducive to oscillations which can be chaotic.

4.5 The Vallis model : accounting for the Bjerkness feedback

The Vallis 1988 model is focused on the consequences of the Bjerkness feedback by conceptualising the connections between horizontal advection, upwelling and surface wind. It includes three variables: West Pacific temperature T_w, East Pacific T_e and surface current speed u.
The latter has relaxation dynamics to a background, trade-wind forced velocity $u^\star$, but modulated by the East-Wast gradient. Then this wind-speed causes upwelling and downlegging causing water exchanges with the deep-water mass of temperature $\bar{T}$. In addition, surface temperatures

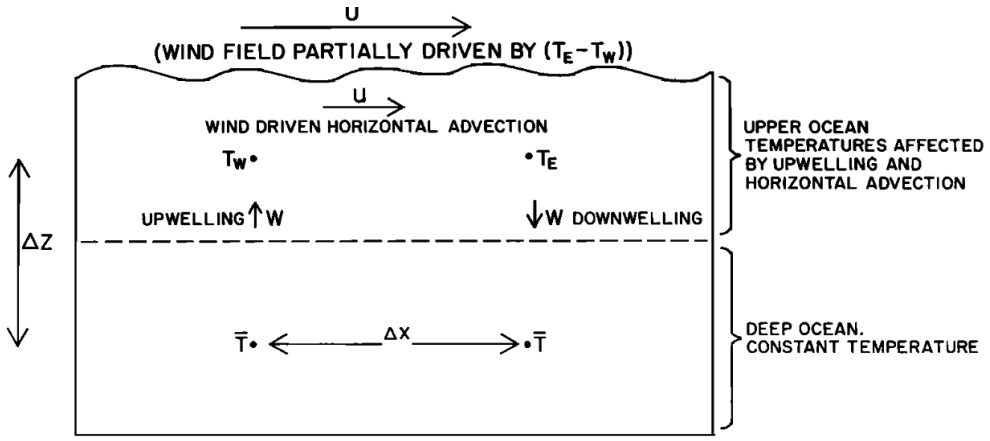

Fig. 1. Schematic diagram of two-point model [after Vallis, 1986].

Figure 4.3: Sketch of the Vallis Model

are relaxed to $T^\star$ (Figure 4.3). This conceptual model then obeys the following equation, assuming a centered advection scheme:

$$\frac{\mathrm{d}u}{\mathrm{d}t} = B\frac{T_e - T_w}{2\delta x} - C(u - u^\star)$$
$$\frac{\mathrm{d}T_w}{\mathrm{d}t} = u\frac{\bar{T} - T_w}{2\delta x} - A(T_w - T^\star)$$
$$\frac{\mathrm{d}T_e}{\mathrm{d}t} = -u\frac{\bar{T} - T_w}{2\delta x} - A(T_e - T^\star)$$

For mathematical analysis, no generality is lost by setting $\bar{T} = 0$ since this only shifts the definition of zero temperature, and temperatures are scaled by $T^\star$. We use $u' = u/(2A\delta x)$ yielding the scaled equations:

$$\frac{\mathrm{d}u'}{\mathrm{d}t} = \alpha(T_e - T_w) - C(u' - u^\star)$$
$$\frac{\mathrm{d}T_w}{\mathrm{d}t} = -u'T_e - A(T_w - 1)$$
$$\frac{\mathrm{d}T_e}{\mathrm{d}t} = u'T_w - A(T_e - 1)$$

The model possesses a symmetric structure around $u^\star$. It features three fixed points. Two of these are associated with well-defined El Niño ($T_e >$

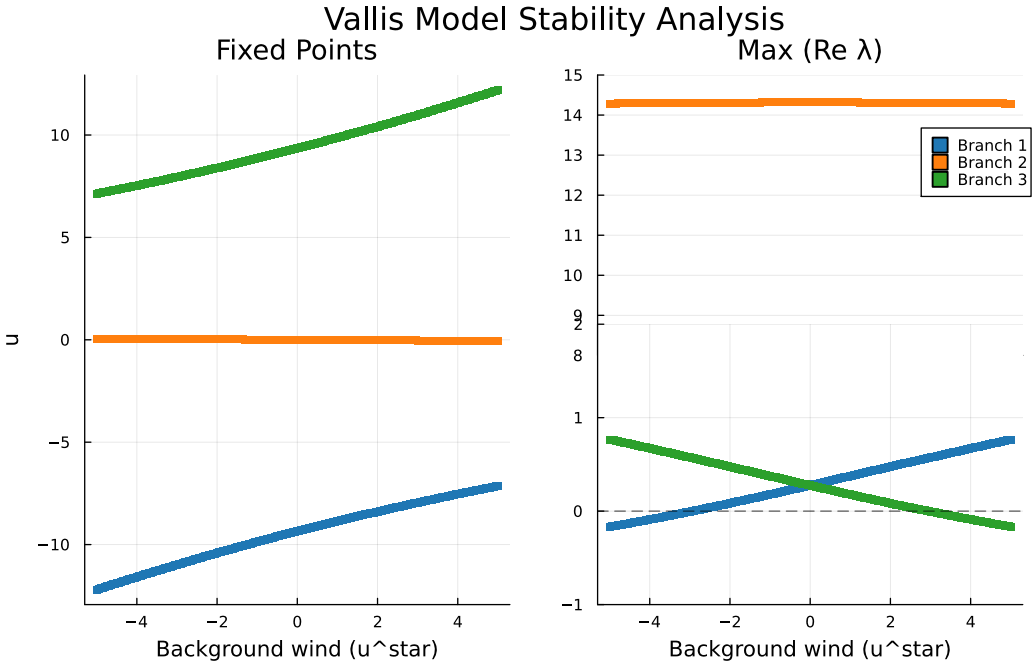

Figure 4.4: Stability analysis of fixed points in the Vallis model

$T_w, u' > 0$) and La Niña ($T_w > T_e, u' < 0$) states, separated by an unstable neutral state. High absolute values of the background wind stress, $u^\star$, stabilize one of these states. These states exchange stability as $u^\star$ shifts between extremes. This is reminiscent of a transcritical scenario, but the transitions are actually governed by Hopf bifurcations. A zone of full instability is bounded by these two Hopf bifurcations, within which trajectories exhibit chaotic behavior. The middle fixed point acts as a saddle point, repelling trajectories along its unstable manifold.
Trajectories near the Hopf bifurcations are fairly complex. Orbits ejected from the unstable points approach a stable point but are not fully captured by it, suggesting the existence of unstable periodic orbits associated with a subcritical Hopf bifurcation. The structural similarity between the Vallis model and the Lorenz 1963 model suggests a shared mechanism for chaos generation: a homoclinic bifurcation. At this specific value of the bifurcation parameter $u^\star$, the unstable manifold loops back to the saddle point, generating a dense set of unstable periodic orbits (see Letellier, Mendes, and Malasoma 2023).
Two remarks:

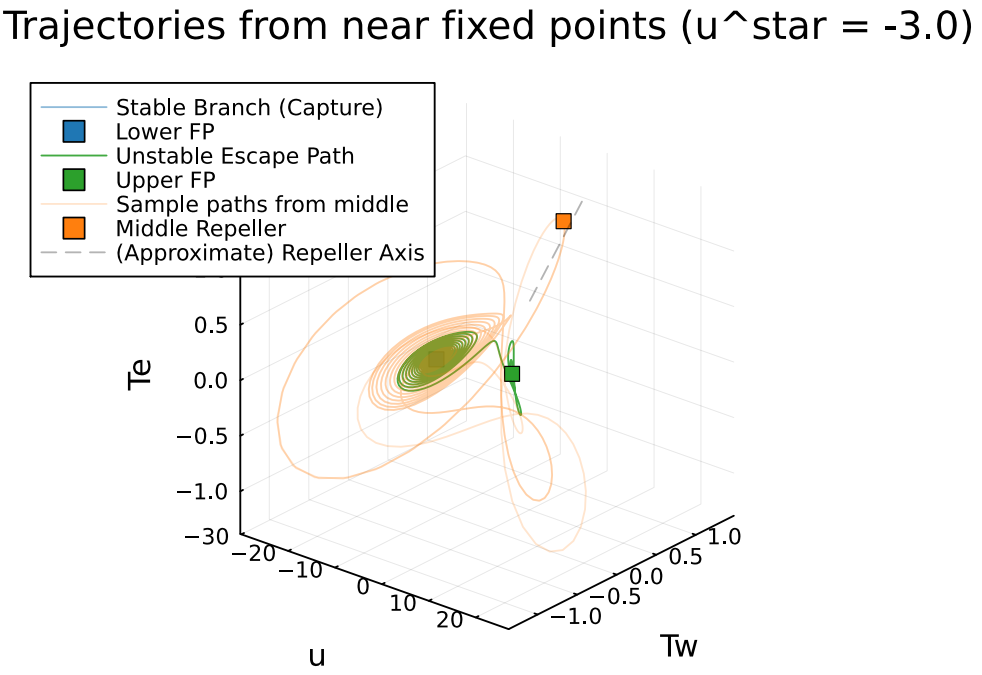

Figure 4.5: Trajectories near the fixed points of the Vallis model : although the left fixed point is stable, trajectories ejected from the unstable fixed points are not captured by it. They are stopped by an unstable orbit (not visible)

- The Vallis model is less frequently cited today and is absent from some key textbooks, such as Dijkstra 2005 and Dijkstra 2013. The Jin 1997 recharge model (see also Timmermann, Jin, and Abshagen 2003; Timmermann, An, et al. 2018) is often preferred because it features thermocline depth explicitly — relying less on horizontal wind velocity. A bifurcation analysis of the Jin model is reserved for future editions of this course (unless you want to do it as an exercise). Yet, the ENSO "bursting" in such systems is likely gated by a homoclinic bifurcation.
- Furthermore, Alexandrov, Bashkirtseva, and Ryashko 2022 has demonstrated that stochastic excitation of a stable fixed point can produce chaotic-like trajectories even in the absence of a global attractor.

4.5.1 The Tziperman madel : chaos and synchronisation accounting for delayed feedbacks

In the Tziperman, Stone, et al. 1994 model, the El Niño-Southern Oscillation (ENSO) is modeled here as a self-sustained delayed oscillator. The dynamics are governed by the interplay of two primary oceanic feedbacks:

- *Positive Feedback (Kelvin Waves):* Represented by the term $bA(h(t-\tau_1))$. Warm anomalies in the central Pacific trigger eastward-propagating Kelvin waves that deepen the thermocline locally, amplifying the initial warming.
- *Negative Feedback (Rossby Waves):* Represented by the term $cA(h(t-\tau_2))$. The same initial anomalies trigger westward-propagating Rossby waves. These reflect off the western boundary as "upwelling" Kelvin waves, eventually returning to the central Pacific to shoal the thermocline and terminate the event.

The evolution of the thermocline depth anomaly $h(t)$ is described by the following Deterministic Delay Differential Equation (DDE):

$$\frac{dh}{dt} = bA(h(t-\tau_1)) - cA(h(t-\tau_2)) - dh(t) + f\cos(\omega t) \tag{4.7}$$

Where:

- τ_1 and τ_2 are the propagation delays for the Kelvin and Rossby wave circuits, respectively.

- d is a linear damping coefficient representing dissipative processes.
- $f\cos(\omega t)$ represents the **seasonal forcing**, with $\omega = 2\pi$ (annual cycle).

The function $A(h)$ represents the non-linear coupling between the thermocline depth and the sea surface temperature (SST). It follows the piecewise formulation of Munnich et al. (1991):

$$A(h,\kappa_0) = \begin{cases} b_m + \frac{b_m}{a_m}\left[\tanh\left(\frac{\kappa_0 a_m}{b_m}(h-h_m)\right) - 1\right] & h < h_m \\ \kappa_0 h & h_m \leq h \leq h_p \\ b_p + \frac{b_p}{a_p}\left[\tanh\left(\frac{\kappa_0 a_p}{b_p}(h-h_p)\right) - 1\right] & h > h_p \end{cases} \tag{4.8}$$

- **Non-linearity (κ_0):** This parameter measures the sensitivity of the atmosphere to oceanic anomalies. Physically, it is tied to the vertical water stratification. A higher κ_0 implies a "stiffer" system where small thermocline changes trigger large SST responses.
- **Saturation (b_m, b_p):** These represent the physical limits of the mixed layer. A very deep or very shallow thermocline eventually "saturates," meaning further displacements no longer produce proportional changes in surface temperature.

4.5.2 Transition to Chaos

By varying κ_0, we observe the transition from a stable limit cycle to frequency locking (Arnold Tongues) and eventually to deterministic chaos. This chaos arises from the competition between the system's intrinsic frequency and the periodic seasonal forcing, leading to the irregular "events" characteristic of the observed ENSO record.
Chaos is not obvious from the figure (attractor seems to be topologically a closed curve, while chaos should generate a strange geometry) but can be confirmed with greatest lyapunov exponent. Chaos is not always spectacular (we will see this later on about climate dynamics).
The Tziperman and Gildor 2003 delayed differential equation model provides three insights:

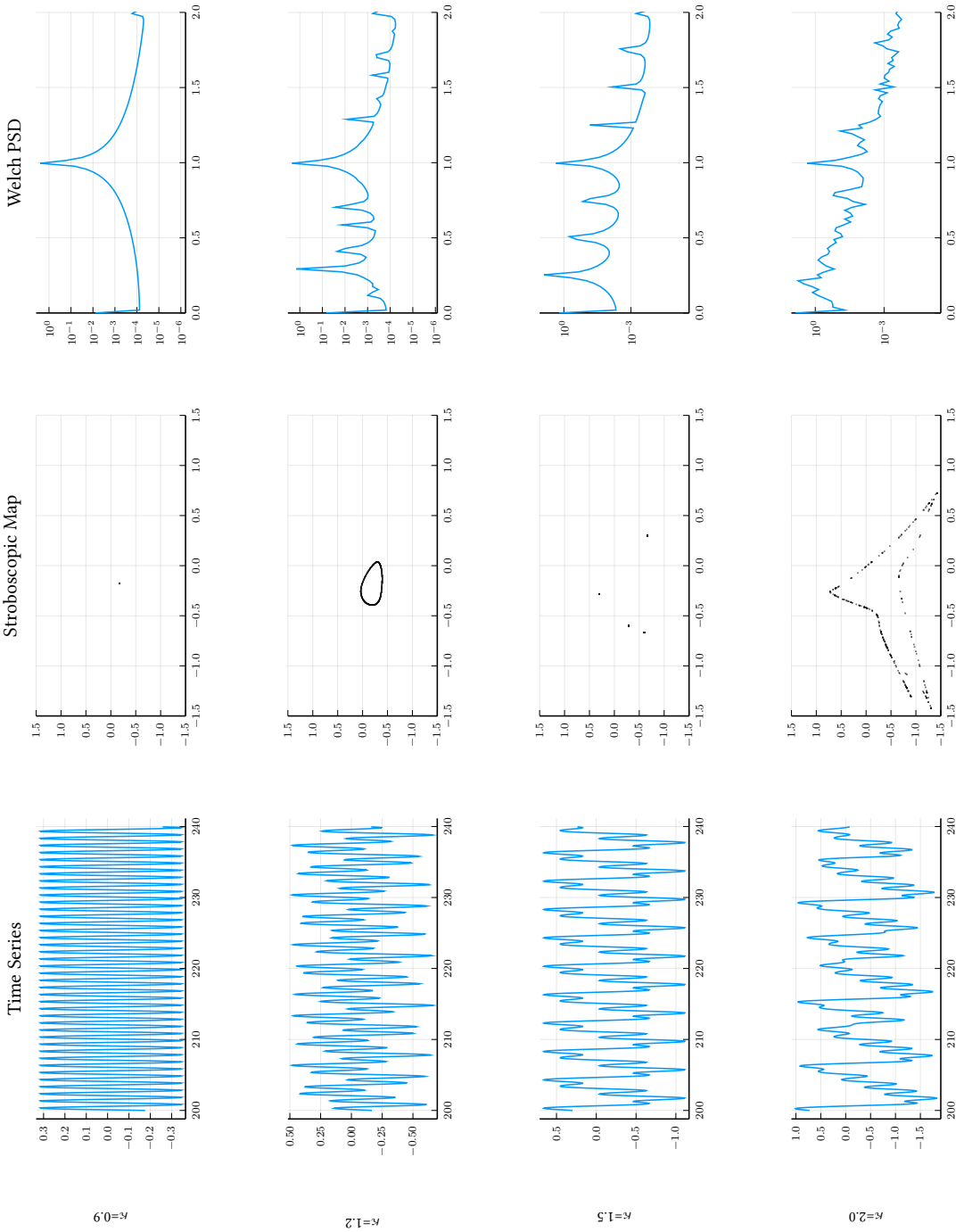

Figure 4.6: The El Niño-Southern Oscillation (ENSO) is modeled as a Delayed Differential Equation (DDE) representing the thermocline depth anomaly h in the eastern Pacific.

- The delayed nature of the feedbacks, associated with the Kelvin and Rossby waves, can introduce a self-sustained oscillation without external forcing. This is not surprising, given that the delayed differential equation has the inherent level of complexity to generate limit cycles, but this is no proof that it should be so in the real world;
- The limit cycle can synchronise with the annual forcing, thus providing a mechanism by which El-Niño and La-Niña events occur about the same time of the year
- Increased coupling strength (κ) causes a transition to chaos via a "period-doubling cascades within overlapping resonance tongues" (Keane, Krauskopf, and Postlethwaite 2016)

In summary, Tziperman, Stone, et al. 1994's model is based on the notion of delayed feedback and it is based on considerations about equatorial waves. Keane, Krauskopf, and Postlethwaite 2016 has investigated the dynamics of this model in depth and found that that asymmetry in the coupling function between the mixed-layer and the surface temperature is particularly important for reproducing characteristic features more realistically. The have confirmed that the chaotic behavior emerges through the emergence of period-doubling cascades within overlapping resonance tongues.

Chapter 5

Non-normal growth

5.1 The alternative paradigm: non-normal stochastic excitation

Several references emphasize (e.g. Dijkstra 2005) that ENSO is fundamentally a 3-D ocean–atmosphere problem that is only grossly captured by ODEs or stochastic ODEs. One paradigmatic reference for a PDE-based ENSO model is the Zebiak and Cane 1987 model. ENSO can also be simulated with more complex models.
The dynamical structure of the system can be reconstructed by inspecting a posteriori observations or simulations with PDE models, following techniques applied, e.g. in Kondrashov and Ghil 2006 and Timmermann, Voss, and Pasmanter 2001. These approaches pay specific attention to stochastic forcing, which brings us to the role that stochastic forcing may play in weakly non-linear systems.
In this context, it has been suggested that actual ENSO dynamics are less non-linear than in the conceptual models proposed, but that non-normal growth excited by stochastic forcing may explain several characteristics of ENSO dynamics (Penland and Sardeshmukh 1995).
We illustrate the principle with the non-normal Stuart–Landau system with stochastic forcing. It is defined by the following pair of coupled stochastic differential equations:

$$\begin{aligned} \mathrm{d}x &= \left(-3x + \delta y - \beta(x^2+y^2)x\right)\mathrm{d}t + \sigma\,\mathrm{d}W_x \\ \mathrm{d}y &= \left(-3y + x/\delta - \beta(x^2+y^2)y\right)\mathrm{d}t + \sigma\,\mathrm{d}W_y \end{aligned} \tag{5.1}$$

where:

- δ is the non-normal coupling parameter responsible for transient growth (normality for $\delta = 1$),
- $\beta > 0$ is the coefficient of the cubic nonlinearity that saturates the growth,
- σ represents the noise intensity, and $\mathrm{d}W_x$, $\mathrm{d}W_y$ are independent Wiener processes.

This model is not derived from actual physics and is used here purely to illustrate the concept of non-normal growth.
Consider first the deterministic part of the system, and more specifically

the linearised system near the origin, which is a fixed point. We have

$$\dot{\boldsymbol{x}} = A\boldsymbol{x}, \quad A = \begin{pmatrix} -3 & \delta \\ 1/\delta & -3 \end{pmatrix}.$$

Matrix A admits two negative real eigenvalues, $\lambda = -2$ and $\lambda = -4$, associated with two eigenvectors $(\delta, 1)$ and $(-\delta, 1)$. Only for $\delta = 1$ are they orthogonal. In the limit of large or small δ, the eigenvectors become nearly colinear, indicating strong non-normality.
We are interested in the behaviour of the norm $\boldsymbol{x}^\dagger\boldsymbol{x}$:

$$\begin{aligned} \frac{\mathrm{d}}{\mathrm{d}t}\boldsymbol{x}^\dagger\boldsymbol{x} &= \frac{\mathrm{d}}{\mathrm{d}t}\boldsymbol{x}^\dagger\boldsymbol{x} + \boldsymbol{x}^\dagger\frac{\mathrm{d}}{\mathrm{d}t}\boldsymbol{x} \\ &= \boldsymbol{x}^\dagger A^\dagger\boldsymbol{x} + \boldsymbol{x}^\dagger A\boldsymbol{x} \\ &= \boldsymbol{x}^\dagger(A^\dagger + A)\boldsymbol{x}. \end{aligned}$$

Consider the gradient:

$$\frac{\partial}{\partial\boldsymbol{x}}\boldsymbol{x}^\dagger(A^\dagger + A)\boldsymbol{x} = 2(A^\dagger + A)\boldsymbol{x}.$$

Maximal instantaneous growth occurs along the eigenvectors of the Hermitian part $\frac{1}{2}(A^\dagger + A)$:

$$(A^\dagger + A) = \begin{pmatrix} -6 & \delta + 1/\delta \\ \delta + 1/\delta & -6 \end{pmatrix}.$$

The eigenvectors are $(1, -1)$ with eigenvalue $-6 - (\delta + 1/\delta)$ (always negative), and $(1, 1)$ with eigenvalue $-6 + (\delta + 1/\delta)$. The latter is positive when

$$\delta + \frac{1}{\delta} > 6,$$

which, for small δ, corresponds to $\delta \lesssim 0.17$. Thus, in this regime, transient growth of the norm occurs near the origin along the direction $(1, 1)$ (or $(-1, -1)$), even though the system is asymptotically stable.
We now consider the stochastic system and rewrite it in polar coordinates. To obtain equations for $\mathrm{d}r$ and $\mathrm{d}\theta$ we use the Itô formula (e.g. Gardiner 2004, eq. 4.3.14):

$$\mathrm{d}f = f_x\,\mathrm{d}x + f_y\,\mathrm{d}y + \frac{1}{2}f_{xx}(\mathrm{d}x)^2 + \frac{1}{2}f_{yy}(\mathrm{d}y)^2 + f_{xy}(\mathrm{d}x\,\mathrm{d}y).$$

We take $r = \sqrt{x^2 + y^2}$ and $\theta = \text{atan2}(y, x)$. After some algebra, one finds:

$$\mathrm{d}r = \left[-3r - r^3 + r\left(\delta + \frac{1}{\delta}\right)\sin\theta\cos\theta + \frac{\sigma^2}{2r}\right]\mathrm{d}t + \sigma\,\mathrm{d}W_r \tag{5.2}$$

$$\mathrm{d}\theta = \frac{1}{2}\left[\left(\frac{1}{\delta} - \delta\right) + \left(\frac{1}{\delta} + \delta\right)\cos(2\theta)\right]\mathrm{d}t + \frac{\sigma}{r}\,\mathrm{d}W_\theta \tag{5.3}$$

The noise term in $\mathrm{d}r$ is

$$\sigma\left(\frac{x}{r}\,\mathrm{d}W_x + \frac{y}{r}\,\mathrm{d}W_y\right),$$

which has variance σ^2 and defines $\mathrm{d}W_r$. Similarly, for θ:

$$\sigma\left(-\frac{\sin\theta}{r}\,\mathrm{d}W_x + \frac{\cos\theta}{r}\,\mathrm{d}W_y\right) = \frac{\sigma}{r}\,\mathrm{d}W_\theta.$$

Since $\mathrm{d}W_x$ and $\mathrm{d}W_y$ are independent, so are $\mathrm{d}W_r$ and $\mathrm{d}W_\theta$.
The equation for $\mathrm{d}r$ shows a "centrifugal" effect induced by stochastic forcing. The term involving $\sin\theta\cos\theta = \frac{1}{2}\sin(2\theta)$ becomes significant when $\delta \ll 1$ or $\delta \gg 1$.
To better understand the behaviour, we adopt a time-scale separation assumption. For small r and neglecting noise, the radial drift is proportional to r. Taking $\beta = 1$, we expect r to remain $O(1)$. The drift term for θ is proportional to δ or $1/\delta$, and for $\delta \ll 1$ it dominates. We therefore assume that θ rapidly samples its stationary distribution, so that:

$$\mathrm{d}r = \left[-3r - r^3 + r\left(\delta + \frac{1}{\delta}\right)\langle\sin\theta\cos\theta\rangle + \frac{\sigma^2}{2r}\right]\mathrm{d}t + \sigma\,\mathrm{d}W_r.$$

We estimate $\langle\sin\theta\cos\theta\rangle$ from the stationary solution of the Fokker–Planck equation associated with (5.3):

$$0 = -\frac{\partial}{\partial\theta}(A\rho) + \frac{1}{2}\frac{\partial^2}{\partial\theta^2}(B\rho), \tag{5.4}$$

where

$$A = \frac{1}{2}\left[\left(\frac{1}{\delta} - \delta\right) + \left(\frac{1}{\delta} + \delta\right)\cos(2\theta)\right], \quad B = \frac{\sigma^2}{r^2}.$$

Following Gardiner 2004, one introduces the probability flux:

$$J = A\rho - \frac{B}{2}\frac{\partial \rho}{\partial \theta}.$$

Defining the potential

$$\Phi(\theta) = -\frac{2}{B}\int_0^\theta A(\theta')\ \mathrm{d}\theta',$$

one obtains the general solution:

$$\rho_\theta(\theta) = e^{-\Phi(\theta)}\left[\rho_\theta(0) + \frac{2J}{B}\int_0^\theta e^{\Phi(\theta')}\ \mathrm{d}\theta'\right]. \tag{5.5}$$

The constant J is determined by imposing periodicity, and $\rho_\theta(0)$ by normalization. The resulting distribution shows that θ lies preferentially near $\pi/4$ and $5\pi/4$, i.e. along directions of transient growth. This implies

$$\frac{1}{2}\langle \sin(2\theta)\rangle \lessapprox \frac{1}{2}.$$

Returning to the drift term for r, the contribution

$$\left(\delta + \frac{1}{\delta}\right)\langle \sin\theta\cos\theta\rangle$$

can outcompete the stabilising term $3r$ when $\delta + 1/\delta > 6$, i.e. for $\delta \lesssim 0.17$. For example, $\delta = 0.08$ lies well within this regime.

The centrifugal drift caused by the time spent in directions of transient growth leads to a depletion of probability near the origin. The nonlinear term $-r^3$ acts as a saturation mechanism, leading to a bimodal radial distribution.

A fuller analysis would require solving the Fokker–Planck equation for r, which is left as an exercise. In this case, $J = 0$ satisfies regularity and $\rho(\infty) = 0$.

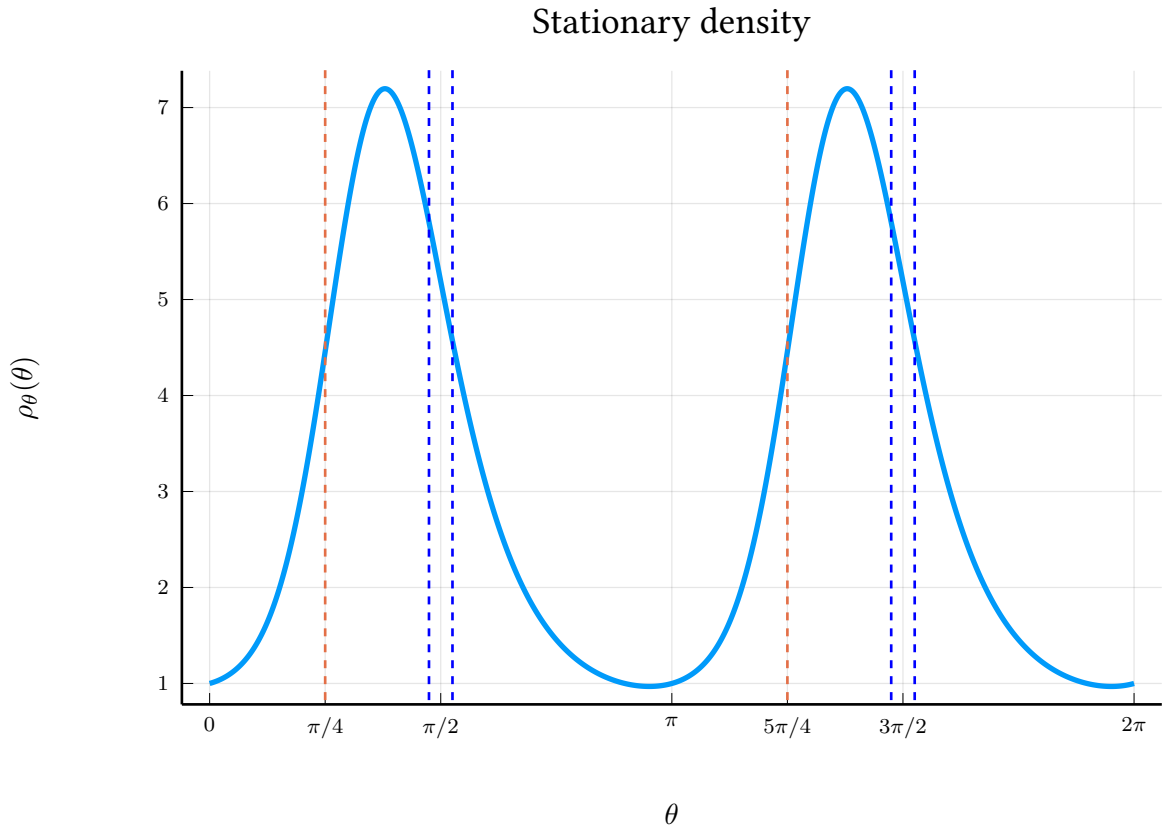

Figure 5.1: Distribution $\rho(\theta)$ obtained from eq. 5.5 with $\sigma = 5$, $r = 2$ and $\delta = 0.08$.

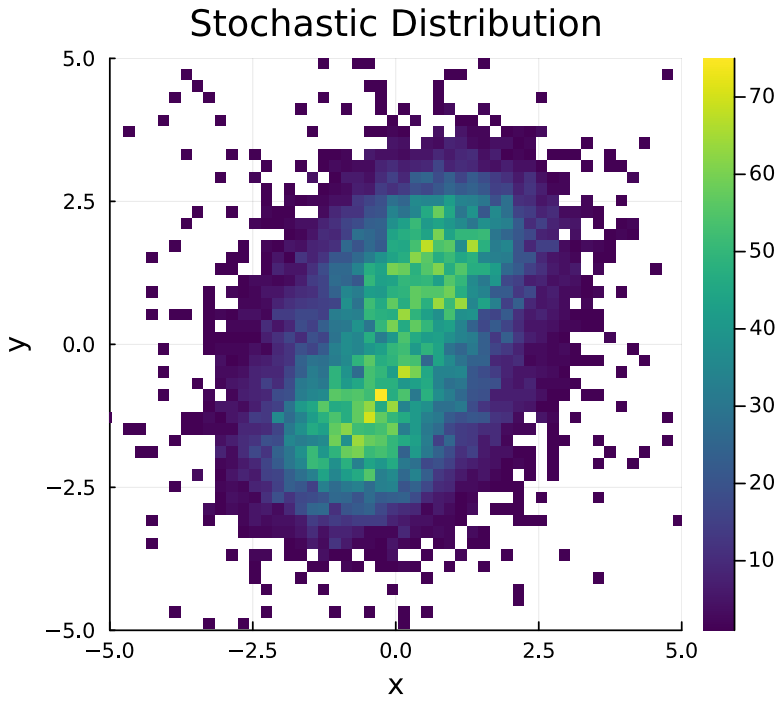

Figure 5.2: Stochastic simulation for $\sigma = 5, \delta = 0.15$. The bimodal distribution is caused by stochastic excitation of non-normal growth.

Chapter 6

Climate dynamics

6.1 Astronomical forcing

6.1.1 Elements of insolation theory

6.1.1.1 Zonal, instantaneous insolation

At time scales ranging from 10^4 to 10^7 years changes in Earth's orbit and inclination which modulate the seasonal and latitudinal distributions of incoming solar radiation. The forcing is referred to as orbital, astronomical or Milankovitch forcing. Milankovitch is the author of the "Canon of insolation" theorising the causal link between astronomical forcing and glaciation.
At any time t the incoming solar radiation, measured in W/m^2, is a product of the Earth-Sun distance and a geometric factor measuring the angle of the Earth sun vector with respect to the Earth' surface. We note the Earth's semi-great axis a, and the Eart distance is $a\rho$. $a\rho$ is obtained with adequate accuracy by application of Keplerian dyanimcs. Let ν the true anomaly measuring the heliocentric angle between the perihelion and Earth, and e (Figure 6.1), the eccentricity of the orbit (e.g. Murray and Dermott 2000, p. 28):

$$\rho = \frac{1 - e^2}{1 + e \cos \nu}$$

The energy receveived by a surafce unit perpendicular to the surface is $W = \frac{S_0}{\rho^2} \cos z$, where S_0 is the solar irradiance at distance a and z the Sun zenith angle. The latter depends on the Sun's hour angle H which marks the diurnal movement. It is obtained by resolution of spherical triangles involving the Sun's declination δ and the observer's geodetic latitude (cf. course LGEO1242):

$$\cos z = \sin \phi \sin \delta + \cos \phi \cos \delta \cos H$$

For averaging over the parallel (line of equale latitudes), one must determine the hour angles at sun set and sunrise. It is generally given by

$$\cos(H_0) = - \tan \phi \tan \delta$$

$\lambda_\odot$	$\lambda_{\overset{+}{\odot}}$	δ	
0	π	0	March equinox
$\pi/2$	$3\pi/2$	ε	June solstice
π	0		September equinox
$3\pi/2$	$\pi/2$	$-\varepsilon$	December solstice

but it is undefined if $\tan\phi\tan\delta < -1$ (polar day) or > 1 (polar night).
Incoming solar radiation averaged an geographic parallel of latitude ϕ is then

$$W_d = \frac{1}{2\pi}\frac{2S_0}{\rho^2}(H_0\sin\phi\sin\delta + \cos\phi\cos\delta\sin H_0) \tag{6.1}$$

with $H_0 = \arccos(-(\max(-1, \min(1, \tan\phi\tan\delta))))$.
The declination δ of the Sun is in a spherical triangle involving the true solar longitude ($\lambda_\odot$, measured on the Celestial sphere) and the obliquity ε (Figure 6.2):

$$\cos\delta = \sin\lambda_\odot\cos\varepsilon. \tag{6.2}$$

Equation 6.2 relates angles on a geocentric celestial sphere, while the Keplerian orbit is rather modelled in heliocentric coordinates. The earth's heliocentric longitude, noted $\lambda_{\overset{+}{\odot}}$ satisfies

$$\lambda_{\overset{+}{\odot}} = \lambda_\odot + \pi = \varpi_\odot + \nu + \pi \tag{6.3}$$

Characteristic longitudes, defining seasons given in Table 6.1.1.1
For example, zonal insolation at June's soltice is

$$\begin{aligned} W_{js} &= \frac{1}{2\pi}\frac{2S_0}{\rho^2}(H_0\sin\phi\sin\varepsilon + \cos\phi\cos\varepsilon\sin H_0) \\ H_0 &= \arccos(-(\max(-1, \min(1, \tan\phi\tan\varepsilon)))) \\ \rho &= \frac{1-e^2}{1+e\sin\varpi_\odot} \end{aligned} \tag{6.4}$$

The thesis by Loutre 1993 provides trigonometrical expansions of insolations. We show in the attached jupyter notebook how to use `maxima` to reproduce some key results. In this case, one finds (with a small angle approximation for obliquity)

$$W_{js} = \frac{S_0}{\pi}\left[\cos\phi + (\frac{\pi}{2}\sin\phi)\varepsilon + \pi e \sin\varpi_{\odot}\sin\phi\right] + \mathcal{O}(e^2) + \mathcal{O}(\varepsilon^2) \quad (6.5)$$

This provides first order dependencies on obliquity and $e\sin\varpi_{\odot}$. The latter parameter is commonly called the Earth climate precession parameter though sign conventions vary and it is also seen defined as $e\sin\varpi_{\oplus} = -e\sin\varpi_{\odot}$.

6.1.1.2 Insolation integrated over time

The true anomaly ν measures the angle between perihelion and the March equinox position. Its dynamics satisfy the conservation of angular momentum (e.g. Murray and Dermott 2000, eq. 2.8), that is the second law of Kepler:

$$a^2\rho^2\frac{\mathrm{d}\nu}{\mathrm{d}t} = L = \sqrt{\mu a(1-e^2)}, \quad (6.6)$$

with $\mu = \mathcal{G}(m_{\odot} + m_{\oplus})$.
It is classically related to other angles marking the Keplerian movement: the mean anomaly M which, by definition, is linear with celestial time, and the eccentricy anomaly (todo: annex). All angles are zero when reaching perihelion. In particular

$$M = n(t-\tau), \quad \text{with } \tau\text{, time of passing at perihelion}$$

By this definition, the revolution period $T = 2\pi/n$. One can also define a *mean longitude* as $\lambda_M = M + \varpi$ (Figure 6.1).
Using the time integral over the Earth revolution one finds that

$$T^2 = \frac{4\pi^2}{n^2} = \frac{4\pi^2}{\mu}a^3,$$

so that the angular momentum conservation (6.6) can be written as

$$\rho^2\frac{\mathrm{d}\nu}{\mathrm{d}t} = n\sqrt{1-e^2} \quad (6.7)$$

As a consequence, the total energy received over two angular positions in the orbit does not involve the Earth-Sun distance over that interval:

$$\int_{\nu_1}^{\nu_2} W_d \, \mathrm{d}t = \int_{\nu_1}^{\nu_2} W_d \frac{\mathrm{d}\nu}{\dot{\nu}}.$$

The equation can be recast in terms of Earth longitudes — which define seasons — via (6.3)

$$\int_{\lambda_1}^{\lambda_2} W_d \, \mathrm{d}t = \frac{S_0}{\pi} \frac{1}{n\sqrt{1-e^2}} \int_{\lambda_1}^{\lambda_2} \left(H_0 \sin\phi \sin\delta + \cos\phi \cos\delta \sin H_0\right) \, \mathrm{d}\lambda. \tag{6.8}$$

Given that δ and H_0 are functions of λ, ϕ and ε, this equation carries an important result:

Key Outcome: Insolation integrated over a season

Total energy received over a season, at any latitude, is independent of the longitude of the perihelion ϖ (be it geocentric or heliocentric).

The $\int_{\lambda_1}^{\lambda_2}$ that appears under (6.8) involves elliptic integrals; details are provided in Berger, Loutre, and Yin 2010. Insolation received over the entire Earth is easier to compute. At any time t the global averaged insolation divided by the full area of the Earth surface satisfies

$$W_g = \frac{1}{4} \frac{a^2}{\rho^2} S_0, \tag{6.9}$$

the $\frac{1}{4}$ factor being the effective section of a sphere. Integration using (6.7) gives:

$$\int_{\lambda_1}^{\lambda_2} a^2 W_g \frac{\mathrm{d}\nu}{\dot{\nu}} = \frac{S_0}{4} \frac{\lambda_2 - \lambda_1}{n\sqrt{1-e^2}}. \tag{6.10}$$

In particular, the global, annual mean insolation averaged over the Earth's revolution time is

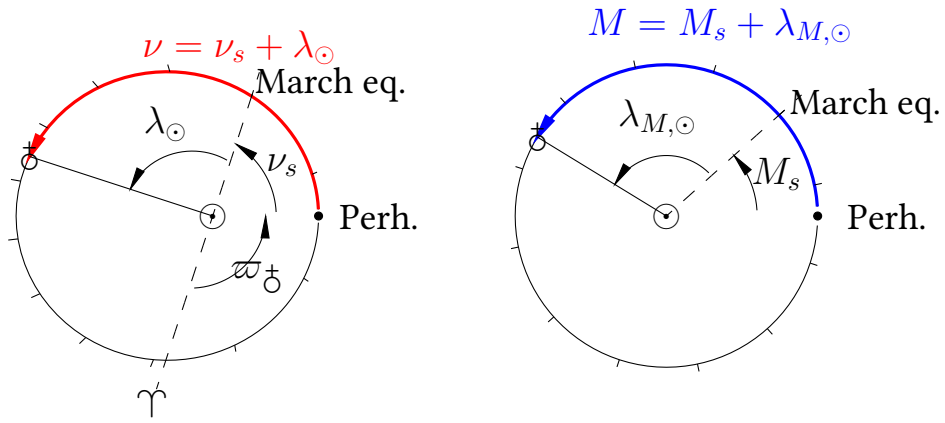

Figure 6.1: The climatic calendar starts with the March equinox, when the Earth and the moving vernal point (ascending node on ecliptic, see Fig 6.2) are aligned, and the true longitude of the Sun λ_{odot} is zero. This is the quantity needed to compute the Sun's declination for a given obliquity. The mean anomaly $M(t)$ measures the time elapsed since the March equinox. The left-hand-side figure provides true angles, and the right-hand-side mean angles, which progress linearly with time. Ticks are equally spaced in times.

$$W_{g,a} = \frac{S_0}{4a^2}\frac{1}{\sqrt{1-e^2}} = \frac{S_0}{4a^2}(1 + \frac{e^2}{2} + \mathcal{O}(e^4))$$

The *mean* energy over a season is affected by the longitude of the perihelion.

6.1.1.3 Which insolation matters for climate

STILL TODO

6.1.2 The planetary problem

This section reviews important results from the Laplace-Lagrange secular theory.
To a restricted approximation, the Earth can be modeled as a test particle in the gravitational field dominated by the Sun and Jupiter. The motion can be framed as a standard problem in classical mechanics, where the integrable Hamiltonian of the two-body problem ($\mathcal{H}_0$) is perturbed

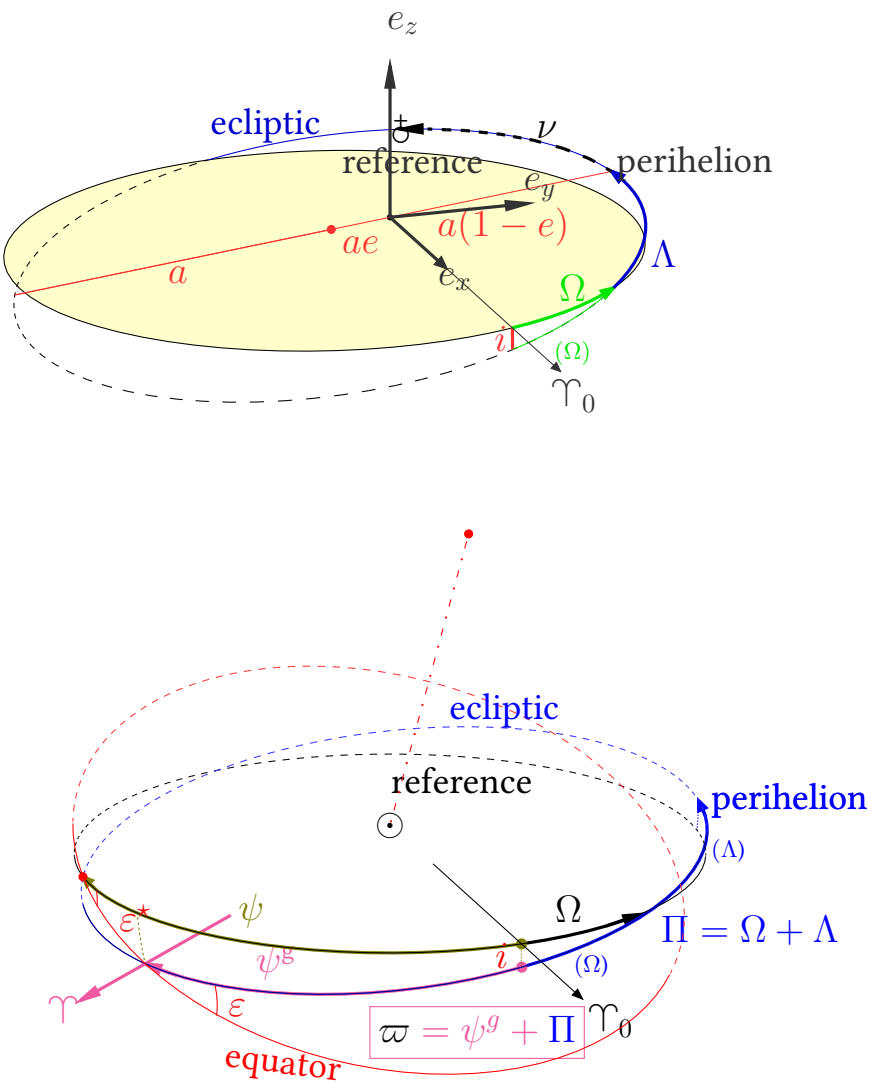

Figure 6.2: (left) orbital elements of Earth positionned with respect to an invariant plane, (right) moving eclipic and equator defining angles relevant for insolation theory. See how ϖ emerges as the sum of Ψ^g and Π.

($\mathcal{H} = \mathcal{H}_0 + \mathcal{H}_1$). This is classically solved via averaging methods: terms associated with the individual revolutions of Earth and Jupiter are averaged out, retaining only the mean effect of Jupiter's orbit on Earth's. Mathematically, this is equivalent to either eliminating terms dependent on $\lambda_M(t)$ —Lagrange's method—or reducing orbits to an average belt with Keplerian density—Gauss' averaging method (CITE MURRAY)
The process yields equations for $\dot{e}$, $\dot{a}$, and $\dot{\Pi}$ (the Lagrange planetary equations). However, it has long been recognized (e.g., Laskar's review TODO cite) that the variables $e\cos\Pi$, $e\sin\Pi$, $\sin i\cos\Omega$, and $\sin i\sin\Omega$ are more theoretically adequate, as they eliminate singularities arising when $e \to 0$ or $i \to 0$. These are defined as:

$$\begin{aligned} k &= e\cos\Pi \qquad & h &= e\sin\Pi \\ q &= \sin i\cos\Omega & p &= \sin i\sin\Omega \end{aligned}$$

The variables k, h, p, q are said to be non-singular canonical. Under perturbation theory for Hamiltonian systems, and assuming Jupiter's influence is sufficiently weak, Earth's orbital elements are expected to exhibit free-motion dynamics in the perturbed potential. To first order:

$$\begin{aligned} \dot{k}_3 &= -A_{33}h_3 \quad \text{and} \quad \dot{h}_3 &&= A_{33}k_3 \\ \dot{q}_3 &= -B_{33}p_3 \quad \text{and} \quad \dot{p}_3 &&= B_{33}q_3 \end{aligned} \tag{6.11}$$

The number 3 is a reference to the Earth being the third planet of the solar system, and the reason for duplicating the index will be clear in the following. At this point of the development, $e_3^2 = h_3^2 + k_3^2$ and $\sin^2 i_3 = q_3^2 + p_3^2$ are constant. These equations can be rewritten with the formalism of complex canonical variables (similar to phasors in electronics). Call $z_3 = k_3 + ih_3$ the eccentricity phaser, then the first set of equations reads $\dot{z}_3 = -iA_{33}z_3$. In both case, we recognise the familiar structure of a linear Hamiltonian harmonic system equivalent to a harmonic oscillator, which is expected precisely because the equations have been established to the first order of perturbation.
Next, we take into account that Jupiter is itself coupled with Saturn; "coupled" meaning that they mutually perturb each other, which leads to an exchange of angular momentum. Calling h_5, k_5 and h_6, k_6 the elements for Jupiter (the fifth planet) and Saturn (the sixth planet), one has the following *coupled* equations:

$$\dot{h}_5 = A_{55}k_5 + A_{56}k_6, \quad \dot{k}_5 = -A_{55}h_5 - A_{56}h_6,$$
$$\dot{h}_6 = A_{65}k_5 + A_{66}k_6, \quad \dot{k}_6 = -A_{65}h_5 - A_{66}h_6,$$

and a similar matrix B for the (p, q) elements. The matrix is dominated by diagonal elements, and we expect that both Jupiter's and Saturn's orbits evolve as a superposition of normal modes associated with the eigenvalues g_5 and g_6. Conventionally, g_5 denotes the eigenfrequency close to A_{55}, i.e., close to the free precession rate of Jupiter under Saturn's perturbation, and g_6 that of Saturn.
Namely, the solution is

$$h_5 = e_{55}\sin(g_5 t + \beta_5) + e_{56}\sin(g_6 t + \beta_6)$$
$$h_6 = e_{65}\sin(g_5 t + \beta_5) + e_{66}\sin(g_6 t + \beta_6)$$

or:

$$z_5 = e_{55}\exp(ig_5 t) + e_{56}\exp(ig_6 t)$$
$$z_6 = e_{65}\exp(ig_5 t) + e_{66}\exp(ig_6 t),$$

The e_{ij} are the components of the eigenvectors of the matrix coupling Saturn and Jupier, scaled such as to satisfy initial conditions. In the Jupiter-Saturn system, the off-diagonal terms are small.
The eigenvalues of the (p, q) system are denoted s_5 and s_6. The latter case is specific because one eigenvalue is zero: the secular inclination dynamics conserve the direction of the total angular momentum vector, so that a rigid rotation of all orbital planes leaves the system invariant. Thus only one non-zero eigenvalue persists.
Expressions for the elements of the matrices A and B are given in Murray and Dermott 2000, Ch. 7, Eqs. 7.9–7.12, as well as in the accompagnying Jupyter notebook.
This movement of Jupiter and Saturn modifies the behaviour of Earth's dynamics, which still can be understood as a superposition of free motion (as in (6.11)) and forced motion. Conserving only the significant influence of Jupiter and neglecting the smaller e_{56} coupling:

$$\dot{h}_3 = A_{33}k + A_{35}e_5 \cos(g_5 t + \beta_5), \tag{6.12}$$
$$\dot{k}_3 = -A_{33}h - A_{35}e_5 \sin(g_5 t + \beta_5), \tag{6.13}$$

which can be rewritten as $\dot{z} = -i(A_{33}z + A_{35}z_5)$.
The solution is

$$h_3 = e_{\text{free}} \sin(g_3 t + \beta_3) - \frac{A_{35}e_{55}}{g_3 - g_5} \sin(g_5 t + \beta_5),$$
$$k_3 = e_{\text{free}} \cos(g_3 t + \beta_3) - \frac{A_{35}e_{55}}{g_3 - g_5} \cos(g_5 t + \beta_5),$$

with, in this case, $g_3 = A_{33}$ and e_{free} set by initial conditions.
This superposition of motions is valid because the involved frequencies are non-resonant (i.e., not simple multiples or fractions of each other), not nearly resonant (small denominator problem) and the forcing is weak. This situation is described by the Kolmogorov–Arnold–Moser (KAM) theorem. The basic principle is that the two-body problem (e.g., Jupiter orbiting the Sun) is integrable: it can be expressed in action-angle variables, with as many invariants (actions) as degrees of freedom (3 in the two-body problem). This integrability is broken in the n-body problem with $n > 2$, but if the perturbation is sufficiently small and does not cause resonances, the motion remains regular and the KAM theorem applies. In practice, this means that the action variables, which are strictly constant in the integrable problem, oscillate slightly around their unperturbed values, analogous to the motion of a pendulum.
At this point we can already prove two important results:

- Earth eccentricity varies in response to the combination of its free and forced movement, with angular velocity $g_3 - g_5$. This is one contributor to the 100-ka signal recognised in geological sediments;
- By further perturbing (6.13) by a smaller, higher frequency signal (e.g. Saturn), the instantaneous frequency, measured by the derivative of the argument of z, varies more when eccentricity is small than when eccentricity is large. This is a result with significant implications in cyclostratigraphy.

Then Mars comes on stage. We would like to write:

$$\dot{h}_3 = -A_{33}k_3 + A_{34}k_4 + A_{35}k_5$$
$$\dot{h}_4 = -A_{44}k_4 + A_{43}k_3 + A_{45}k_5$$

Simulating this system will reveal alarming variations in Mars's eccentricity, well beyond the observed range (up to 0.2). What is wrong ?
Mars lives in a gravitational environment that is not that different from Earth, bathed by the remote and substantial influence of Jupiter and Saturn. Hence, unsurprisingly, it has a free motion that is not very different from Earth's. In other words, A_{33} and A_{44} are close to each other. Physically, one might say that Mars and Earth fight each other in their relationship with the angular momentum of Mars. Mathematically, the coupled Earth-Mars system will be characterised by two similar eigenvalues, meaning that their movements will be strongly coupled. Because eigenvalues g_3 and g_4 are so close to each other, amplitudes will be affected by a "small divisor" problem, with, in this linear setting, explains the exuberant variations of e_4.
In the real world this does not occur because non-linear terms "de-tune" the coupling. One simple way to illustrate in a way that is roughly adequate with respect to the full theory is

$$g_3^\star = g_3 + \beta_{\text{self}} e_3^2 + \beta_{\text{cross}} e_4^2$$
$$g_4^\star = g_4 + \beta_{\text{cross}} e_3^2 + \beta_{\text{self}} e_4^2$$

and then

$$\dot{h}_3 = -g_3^\star k_3 + A_{34}k_4 + A_{35}k_5 \dot{h}_4 \qquad = -g_4^\star k_4 + A_{43}k_4 + A_{45}k_5$$

We see that this system differs from the linear one by the presence of non-linear terms in the free term (β_{free}) and in the interactions β_{cross}). In the accompagnying Python notebook, we suggest $\beta_{\text{cross}} = 0.3\beta_{\text{free}}$.

Play with chaos

1. Take the Python notebook and observe how subtle changes in β_{free} trigger transitions between chaotic and quasi-periodic regimes. Larger values of β_{free} detune the near-resonance between Earth and Mars, leading to orbits confined to bounded ranges comparable to observed eccentricities. Smaller values of β_{free} allow for intermittent resonance overlap, which is a mechanism for the onset of Hamiltonian chaos.
2. Then, review the Laskar, Joutel, and Boudin 1993 and Laskar, Fienga, et al. 2011 studies and comment on the role of inclinations

6.1.3 The luni-solar precession

Introduction of general precession Ψ_g. definition of climate-relevant elements: $e \sin \varpi$, $e \cos \varpi$.
explain forcing = multiple frequencies

6.1.4 The climate modelling problem

ice and carbon cycle generate non-linear dynamics forced by multiple frequencies

- non-linearity via rectification
- via period doubling scenario
- via synchronisation of limit cycle
- via stochastic excitation

- long-range fluctuations in an EMBM

Index

annual cycle, 15
attractor, 11
averaging methods, 100
averaging regime, 10, 11

baroclinic, 40
barotropic, 36, 40
Bernoulli equation, 35
Bjerknes feedback, 15
Boussinesq approximation, 38
Brownian motion, 8
Brunt-Väisälä frequency, 38
buoyancy frequency, 38

capillary effects, 35
chaos, 15
classical mechanics, 98
climate precession parameter, 96
climatic calendar, 98
conservation of potential vorticity, 43

daily cycle, 15
declination, 98
deterministic chaos, 82
dispersion relation, 37
diurnal cycle, 15

eccentricity, 15
El Niño-Southern Oscillation (ENSO), 15
elliptic integrals, 97
Euler equation, 38
excitable dynamics, 15
external forcings, 15

finite-memory, 9
fluctuating regime, 11
fluctuation spectrum, 10
Fokker–Planck equation, 88
forced oscillations, 15
frequency locking, 82

glacial-interglacial cycles, 15
Gravity waves, 34
grows with the scale, 10

Hamiltonian, 98
Hasselmann's theory, 13

insolation, 97
internal gravity waves, 38
Itô formula, 87

Kelvin waves, 15

Lagrange planetary equations, 100
Laplace equation, 36

limit cycles, 15
linear energy balance model, 15
linear theory, 13
low-order dynamical systems, 15

macro-climate, 11
macro-weather, 11
mean anomaly, 98

non-normal growth, 86
non-stationary, 8, 9
nonlinear concepts, 16
nonlinear dynamics, 15
nonlinear internal dynamics, 15
nonlinear resonance, 15, 16

obliquity, 15, 95
Ornstein-Uhlenbeck, 9, 13

periodic, 15
perturbation theory, 100
physical considerations, 15
positive feedback, 15
potential vorticity, 43
power spectrum approach, 16
power spectrum density, 16
precession, 15

quasiperiodic changes, 15
quasiperiodic patterns, 15

reduced gravity, 40
Rossby radius
    Internal, 67
Rossby waves, 15

seiches, 42
static stability parameter, 67
stationary process, 9
stochastic process, 8
synchronization, 15, 16
synoptic waves, 66

test particle, 98
transient growth, 86
two-body problem, 98

velocity potential, 36

wavenumber, 41
weather, 11
Wiener process, 8